Patrick Grahn

Multipole excitations in optical meta-atoms

School of Electrical Engineering

Thesis submitted for examination for the degree of Master of Science in Technology.

Espoo 19.3.2012

Thesis supervisor:

Prof. Matti Kaivola

Thesis instructor:

D.Sc. (Tech.) Andriy Shevchenko

Aalto University
School of Electrical
Engineering

AALTO UNIVERSITY
SCHOOL OF ELECTRICAL ENGINEERING

ABSTRACT OF THE
MASTER'S THESIS

Author: Patrick Grahn

Title: Multipole excitations in optical meta-atoms

Date: 19.3.2012 Language: English Number of pages:7+57

Department of Applied Physics

Professorship: Optics and Molecular Materials Code: Tfy-125

Supervisor: Prof. Matti Kaivola

Instructor: D.Sc. (Tech.) Andriy Shevchenko

Recent developments in nano-optics and nanofabrication technology have made it possible to construct artificial atoms, called meta-atoms, and out of them compose materials with extraordinary optical properties. These materials are called optical metamaterials. Conventionally, meta-atoms are made of noble metals and have their shapes designed to promote certain types of optically excited electric currents. In this thesis, we develop a multipole theory that enables us to exactly identify the excitation character in an arbitrary meta-atom. We propose a new meta-atom design, the disc metadimer, and use our multipole theory to analyze its properties. In contrast to natural atoms, incident light can interact with this meta-atom without exciting any electric dipole moment. Instead, the light excites pronounced magnetic dipole and electric quadrupole moments. We anticipate that a new type of metamaterial, the quadrupole metamaterial, can be constructed of these meta-atoms.

Keywords: metamaterials, multipole expansion, electric quadrupole

AALTO-UNIVERSITETET
HÖGSKOLAN FÖR ELEKTROTEKNIK

SAMMANDRAG AV
DIPLOMARBETE

Författare: Patrick Grahn

Titel: Multipolexcitationer i optiska metaatomer

Datum: 19.3.2012 Språk: Engelska Sidantal:7+57

Institutionen för tillämpad fysik

Professur: Optik och molekylära material Kod: Tfy-125

Övervakare: Prof. Matti Kaivola

Handledare: TkD Andriy Shevchenko

Den senaste utvecklingen inom nanooptik och nanotillverkning har möjliggjort framställning av artificiella atomer som kallas metaatomer. Utav dem kan man framställa material med enastående optiska egenskaper. Dessa material kallas för optiska metamaterial. Metaatomer är vanligtvis framställda av ädelmetaller och är formade så att de främjar specifika optiskt exciterade elektriska strömmar. I denna avhandling utvecklar vi en multipolteori med vilken vi kan exakt identifiera excitationstypen i en godtycklig metaatom. Vi presenterar skivmetadimern, en ny metaatomdesign vars egenskaper vi analyserar med vår multipolteori. I motsats till naturliga atomer så kan inkommande ljus växelverka med denna metaatom utan att excitera elektriska dipolmoment. Istället exciterar ljuset avsevärda magnetiska dipolmoment och elektriska kvadrupolmoment. Vi förutser att dessa metaatomer kan användas för att framställa en ny typ av metamaterial som vi benämner kvadrupolmetamaterial.

Nyckelord: metamaterial, multipolutveckling, elektrisk kvadrupol

Contents

Symbols, operators and special functions

Symbols

$\mathbf{A}$	vector potential
$\mathbf{B}$	magnetic flux density
C_a	absorption cross section
C_{ext}	extinction cross section
C_s	scattering cross section
C_s^e	electric dipole scattering cross section
C_s^m	magnetic dipole scattering cross section
C_s^q	electric quadrupole scattering cross section
$\mathbf{D}$	electric displacement
$\mathbf{E}$	electric field
$\mathbf{E}_F$	electric far-field
$\mathbf{E}_i$	electric field of incident light
$\mathbf{E}_s$	electric field of scattered light
$\mathbf{H}$	magnetic field
$\mathbf{H}_i$	magnetic field of incident light
$\mathbf{H}_s$	magnetic field of scattered light
I_0	intensity of a plane wave
$\mathbf{I}$	electric current
$\overleftrightarrow{\mathbf{I}}$	unit dyadic
$\mathbf{J}$	macroscopic current density
$\mathbf{J}_{c.e.}$	spatially averaged conduction electron current density
$\mathbf{J}_F$	free current density
$\mathbf{J}_S$	source current density
$\mathbf{M}$	magnetization
$\overleftrightarrow{\mathbf{M}}^{(l)}$	current multipole moment of order l
$\mathbf{P}$	electric polarization
$\overleftrightarrow{\mathbf{Q}}$	electric quadrupole moment density
$\overleftrightarrow{\mathrm{Q}}$	current quadrupole moment
$\mathbf{S}$	Poynting vector
W_a	energy absorption rate
W_{ext}	energy extinction rate
W_s	energy scattering rate
a_E	electric multipole coefficient
a_M	magnetic multipole coefficient
$\mathbf{b}$	microscopic magnetic flux density
c	speed of light in vacuum $= 299,792,458$ ms^{-1}
$\mathbf{e}$	microscopic electric field
$\mathbf{j}_m$	microscopic current density
k	wave number $= 2\pi\lambda^{-1}$
$\mathbf{k}$	wave vector

$\mathbf{m}$	magnetic dipole moment
$\mathbf{p}$	electric dipole moment
q	electric charge
$\overleftrightarrow{\mathbf{q}}$	electric quadrupole moment
$\mathbf{r}$	position
t	time
$\mathbf{v}$	velocity
α	electric dipole polarizability
$\overleftrightarrow{\epsilon}$	electric permittivity dyadic
ϵ_0	electric permittivity in vacuum $= \mu_0^{-1} c^{-2}$
ϵ_r	relative electric permittivity
η	wave impedance within medium
λ	wavelength within medium
λ_0	wavelength within vacuum
$\overleftrightarrow{\mu}$	magnetic permeability dyadic
μ_0	magnetic permeability in vacuum $= 4\pi \times 10^{-7}$ Nm^{-2}
μ_r	relative magnetic permeability
ρ	macroscopic charge density
ρ_F	free charge density
$\rho_{c.e.}$	spatially averaged conduction electron charge density
ρ_m	microscopic charge density
$\overleftrightarrow{\sigma}$	conductivity dyadic
$\overleftrightarrow{\upsilon}$	dynamic permittivity dyadic
$\overleftrightarrow{\chi}_e$	electric susceptibility dyadic
$\overleftrightarrow{\chi}_m$	magnetic susceptibility dyadic
ω	angular frequency

Operators

$<>$	spatial average operator
$\cdot$	dot product
$\times$	vector product
E_x	x-component of the vector $\mathbf{E}$
Q_{xy}	element of a dyadic $= \hat{\mathbf{x}} \cdot \overleftrightarrow{\mathbf{Q}} \cdot \hat{\mathbf{y}}$
a^*	complex conjugate of a
$\mathbf{ab}$	outer product between vectors $\mathbf{a}$ and $\mathbf{b}$ (produces dyadic)
$\hat{\mathbf{x}}$	unit vector along the x-axis
∇	nabla operator
$\mathrm{Re}\{a\}$	real part of a
$\mathrm{Im}\{a\}$	imaginary part of a
$\frac{\mathrm{d}}{\mathrm{d}t}$	differentiation with respect to variable t
$\sum$	summation
$\int f(t)dt$	integration of function f over t
$\int f(\mathbf{r})d^3r$	volume integral of function f over all three-dimensional space
$\int f(\theta,\phi)d\Omega$	integration over the solid angle $= \int_0^{2\pi}\int_0^{\pi} f(\theta,\phi)\sin\theta d\theta d\phi$

Special functions

$\mathbf{M}_{lm}$	first solenoidal vector wave function of degree l and order m
$\mathbf{N}_{lm}$	second solenoidal vector wave function of degree l and order m
P_l^m	associated Legendre polynomial of degree l and order m
$\mathbf{X}_{lm}$	vector spherical harmonic of degree l and order m
Y_{lm}	spherical harmonic of degree l and order m
$h_l^{(1)}$	spherical Hankel function of the first kind of order l
$h_l^{(2)}$	spherical Hankel function of the second kind of order l
j_l	spherical Bessel function of order l
n_l	spherical Neumann function of order l
Ψ_l	first Riccati-Bessel function. $\Psi_l(x) = xj_l(x)$
χ_l	second Riccati-Bessel function. $\chi_l(x) = xn_l(x)$
$\delta(x)$	one-dimensional Dirac delta function
$\delta(\mathbf{r}-\mathbf{r}')$	three-dimensional Dirac delta function $= \delta(x-x')\delta(y-y')\delta(z-z')$
$\delta(\mathbf{r})$	three-dimensional Dirac delta function at origin $= \delta(r)/(4\pi r^2)$
δ_{mn}	Kronecker's delta
ξ_l	third Riccati-Bessel function $\xi_l(x) = xh_l^{(1)}(x)$
π_{lm}	second angle-dependent function $\pi_{lm}(\theta) = \frac{m}{\sin\theta}P_l^m(\cos\theta)$
τ_{lm}	first angle-dependent function $\tau_{lm}(\theta) = \frac{d}{d\theta}P_l^m(\cos\theta)$

1 Introduction

In the field of classical optics, propagation of light in homogeneous media is described by the macroscopic Maxwell equations. When the light wave is incident on a boundary between two homogeneous media of different optical properties, it splits into two waves with certain amplitudes, phases and propagation directions. The electromagnetic boundary conditions can be used to solve for these transmitted and reflected waves. However, in deriving these conditions, it is commonly assumed that the electromagnetic field only excites electric and magnetic dipole moments in the atoms or molecules of the medium. Furthermore, at optical frequencies, the magnetization (magnetic dipole moment per unit volume) of most materials is negligibly small. In such cases, light-matter interaction is treated within the electric dipole approximation. To describe certain optical effects, such as optical activity and magnetoelectric effect, the dipole approximation can no longer be used [1]. One then needs to assign higher order electric and magnetic multipoles to the medium. These higher order multipoles not only alter the light wave propagation, but also change the electromagnetic boundary conditions [2, 3]. Therefore, to be able to describe media of this type or, e.g., design new, higher-order optical materials, it is of importance to study the general properties of the multipole excitations that can take place in the elementary constituents of the medium.

Recent developments in nanotechnology have made it possible to construct electromagnetically homogeneous composite materials with designed electromagnetic properties by nano- or microstructuring the constituent materials [4]. These metamaterials exhibit extraordinary electromagnetic phenomena, such as negative refraction and phase velocity [5, 6]. One of the basic elements of a metamaterial with a tailored magnetic response to the electromagnetic field is a metallic split-ring resonator, in which the field can excite a magnetic dipole moment [7]. However, at visible light frequencies, the limited conductivity of metals was found to prohibit efficient excitation of magnetic dipole moments in these resonators [8]. Since then, different structures, such as pairs of cut-wires and plates [9], paired nanopillars [10], fishnet structures [11] and various arrangements of spherical particles [12–14] have been studied in attempts to realize magnetic metamaterials in the spectral range of visible light.

Recently, it was realized that in a metal dimer structure one can optically excite a significant electric quadrupole moment [15]. It was argued that the effective magnetic permeability of a metamaterial can be adjusted also through these electric quadrupole excitations. Thus, the electric quadrupole moment can be the key to unlocking extraordinary electromagnetic phenomena at visible frequencies. In fact, various optical phenomena attributed to the multipole excitations can be found also in natural materials [1]. We therefore predict that by carefully designing a metamaterial that supports resonant multipole excitations, one can enhance these phenomena and, in addition, discover and realize new phenomena. However, a systematic treatment of multipole excitations in artificial structures is still missing in the literature. The goal of this thesis is to develop such a systematic analysis.

Numerical techniques to solve the Maxwell equations can be efficiently used to study the interaction of light with individual sub-units of a metamaterial, which we call meta-atoms. Our goal is to apply numerical calculations to the problem of comprehensive analysis of electromagnetic multipole excitations in each meta-atom, and use the obtained information to determine the light interaction with the metamaterial as a whole. To be able to do this, we first analyze excited electric current distributions in single meta-atoms and decompose them into multipole moments. This allows us to determine the influence of the meta-atom shape on the excitable multipole moments. In particular, we search for optical meta-atoms in which the magnetic dipole and electric quadrupole moments can be significant. We also study the possibility to construct a metamaterial with a significantly reduced electric dipole response, such that the interaction between light and meta-atoms will essentially be determined by higher order multipole moments.

This thesis is organized as follows: In Sec. 2, we describe the basic properties of multipole moments in view of their influence on macroscopic electromagnetic properties of media. We also introduce a multipole expansion that enables one to decompose an arbitrary electromagnetic radiation into electromagnetic fields radiated by electromagnetic multipoles. In Sec. 3, we analyze optical excitations of multipole moments in meta-atoms. By developing a multipole theory we also uncover the main features of the electric current distributions in certain multipole excitations and the means by which the multipole moments can be excited in meta-atoms of certain geometries. In Sec. 4, we use the developed multipole theory to numerically analyze visible light excitations in meta-atoms. We introduce a new meta-atom nanostructure in which the electric quadrupole and magnetic dipole excitations dominate the light-matter interaction. In Sec. 5, we summarize the performed research and present the most important conclusions.

2 The multipole expansion in electromagnetism

In this section, we present the basics of electromagnetism in regard to electromagnetic multipole moments. Several important points related to metamaterials are made throughout the text. We start this section by showing how the multipole moments in molecules appear in the microscopic Maxwell equations and contribute to their macroscopic counterparts. Then we present the constitutive relations providing the connection between the macroscopic sources and electromagnetic fields. We proceed to discuss the electromagnetic boundary conditions that describe the behavior of electromagnetic fields at a boundary between different media. Finally, we introduce our multipole expansion, which is the key working tool of this thesis.

2.1 Maxwell equations

The electromagnetic fields generated by electrically charged particles in vacuum are described by the microscopic Maxwell equations. In SI units the equations may be expressed as

$$\nabla \cdot \mathbf{e}(\mathbf{r},t) = \frac{\rho_m(\mathbf{r},t)}{\epsilon_0}, \tag{1}$$

$$\nabla \cdot \mathbf{b}(\mathbf{r},t) = 0, \tag{2}$$

$$\nabla \times \mathbf{e}(\mathbf{r},t) = -\frac{d\mathbf{b}(\mathbf{r},t)}{dt}, \tag{3}$$

$$\nabla \times \mathbf{b}(\mathbf{r},t) = \frac{1}{c^2}\frac{d\mathbf{e}(\mathbf{r},t)}{dt} + \mu_0 \mathbf{j}_m(\mathbf{r},t). \tag{4}$$

Equations (1)-(4) describe the microscopic electric field $\mathbf{e}$ and the microscopic magnetic flux density $\mathbf{b}$ generated by the microscopic charge density ρ_m and microscopic current density $\mathbf{j}_m$. These four quantities are functions of time and position in the three-dimensional space. The physical constants ϵ_0, μ_0 and $c = 1/\sqrt{\epsilon_0\mu_0}$ are the electric permittivity in vacuum, the magnetic permeability in vacuum and the speed of light in vacuum, respectively.

Matter may be seen to consist of discrete charged particles. Because of this discrete nature of matter, the microscopic quantities are not smooth functions of position. As a consequence, they are usually spatially averaged. The averaging is performed over volumes being large enough for the averaged quantities, $< \rho_m >$ and $< \mathbf{j}_m >$, to be smooth functions of space and time. However, the dimensions of these volumes should be much smaller than the length scale of the spatial variations of $< \mathbf{e} >$ and $< \mathbf{b} >$, which we are interested in. For example, if one is interested in the propagation of electromagnetic waves inside a medium, then the lengths of the averaging volume should be much smaller than the wavelength.

One may consider matter to consist of two kinds of electrically charged particles. First, there are elementary particles that are bound together into well-defined clusters. These clusters we call molecules. Second, there can be unbound conduction electrons in the medium which are not localized to a certain molecule. The former kind of particles are confined to volumes much smaller than the averaging volume.

As a consequence, each molecule may be seen as a point particle. Multipole moments are assigned to the molecules for describing their internal charge and current distributions.

Let a certain l'th molecule have its center of mass at the position $\mathbf{r}_l$. The velocity of the center of mass is $\mathbf{v}_l$. The molecule may have a net charge

$$q_l = \sum_{j(l)} q_j, \tag{5}$$

an electric dipole moment

$$\mathbf{p}_l = \sum_{j(l)} q_j(\mathbf{r}_j - \mathbf{r}_l), \tag{6}$$

an electric quadrupole moment

$$\overleftrightarrow{\mathbf{q}}_l = \frac{1}{2}\sum_{j(l)} q_j(\mathbf{r}_j - \mathbf{r}_l)(\mathbf{r}_j - \mathbf{r}_l), \tag{7}$$

and a magnetic dipole moment

$$\mathbf{m}_l = \frac{1}{2}\sum_{j(l)} q_j(\mathbf{r}_j - \mathbf{r}_l) \times (\mathbf{v}_j - \mathbf{v}_l), \tag{8}$$

where we sum over each elementary particle j in the molecule. In Eqs. (5)-(8), $\mathbf{r}_j$ is the position, $\mathbf{v}_j$ is the velocity and q_j is the charge of the j'th particle. Higher order electric and magnetic moments are less significant and, for simplicity, can be neglected. Equation (8) is classical, and as such, only accounts for the orbital magnetic moment of the molecule. One can also add the contribution of the elementary particles' spins to the magnetic dipole moment. In general, quantum mechanical calculations are needed in order to determine the real multipole moments of the individual molecules.[16]

Next we consider the unbound conduction electrons. The charge density and current density corresponding to these particles are accounted for separately. It is done by adding the averaged conduction electron charge density $\rho_{c.e.}$ and the averaged conduction electron current density $\mathbf{J}_{c.e.}$ to the averages of the corresponding molecular quantities. In a medium that does not move, such that the molecules may be assumed to have zero velocities, the total averaged charge density $\rho =< \rho_m >$ and current density $\mathbf{J} =< \mathbf{j}_m >$ become [16]

$$\rho(\mathbf{r},t) = \rho_F(\mathbf{r},t) - \nabla\cdot\mathbf{P}(\mathbf{r},t) + \nabla\cdot\Big(\nabla\cdot\overleftrightarrow{\mathbf{Q}}(\mathbf{r},t)\Big), \tag{9}$$

$$\mathbf{J}(\mathbf{r},t) = \mathbf{J}_F(\mathbf{r},t) + \frac{d}{dt}\big(\mathbf{P}(\mathbf{r},t) - \nabla\cdot\overleftrightarrow{\mathbf{Q}}(\mathbf{r},t)\big) + \nabla\times\mathbf{M}(\mathbf{r},t), \tag{10}$$

where ρ_F is the free charge density, $\mathbf{J}_F$ the free current density, $\mathbf{P}$ the electric polarization, $\mathbf{M}$ the magnetization and $\overleftrightarrow{\mathbf{Q}}$ the quadrupole moment density. These

five quantities are macroscopic characteristics of the medium and are obtained as [16]

$$\rho_F(\mathbf{r},t) =< \sum_l q_l(t)\delta(\mathbf{r}-\mathbf{r}_l) > +\rho_{c.e.}(\mathbf{r},t), \tag{11}$$

$$\mathbf{J}_F(\mathbf{r},t) = \mathbf{J}_{c.e.}(\mathbf{r},t), \tag{12}$$

$$\mathbf{P}(\mathbf{r},t) =< \sum_l \mathbf{p}_l(t)\delta(\mathbf{r}-\mathbf{r}_l) >, \tag{13}$$

$$\mathbf{M}(\mathbf{r},t) =< \sum_l \mathbf{m}_l(t)\delta(\mathbf{r}-\mathbf{r}_l) >, \tag{14}$$

$$\overleftrightarrow{\mathbf{Q}}(\mathbf{r},t) =< \sum_l \overleftrightarrow{\mathbf{q}}_l(t)\delta(\mathbf{r}-\mathbf{r}_l) >, \tag{15}$$

where the summation is performed over all molecules in the medium. In a metal, the first term in Eq. (11) describes the positively charged ions, whereas the second term describes the negatively charged ensemble of conduction electrons. Notice that, whereas both the ions and the conduction electrons contribute to ρ_F, only the conduction electrons contribute to $\mathbf{J}_F$ as the ions are assumed to be spatially fixed.

In most natural materials $\overleftrightarrow{\mathbf{Q}}$ can be neglected in Eqs. (9) and (10), since usually its contribution to the electromagnetic interaction effects is smaller than that of $\mathbf{P}$ [17]. Also, at optical frequencies, the contribution of $\mathbf{M}$ to ρ and $\mathbf{J}$ is negligibly small compared to the contribution of $\mathbf{P}$ [18]. However, the magnetic dipole moment and electric quadrupole moment are both required in order to describe certain specific optical effects, such as optical activity; even higher order moments, such as magnetic quadrupole and electric octopole moments, are required to explain some electromagnetic phenomena.[1, 2]

Now we take the average of Eqs. (1)-(4) and insert into them the expressions in Eqs. (9) and (10). As a result, we obtain the macroscopic Maxwell equations:

$$\epsilon_0\nabla\cdot\mathbf{E}(\mathbf{r},t) = \rho_F(\mathbf{r},t) - \nabla\cdot\mathbf{P}(\mathbf{r},t) + \nabla\cdot\Big(\nabla\cdot\overleftrightarrow{\mathbf{Q}}(\mathbf{r},t)\Big), \tag{16}$$

$$\nabla\cdot\mathbf{B}(\mathbf{r},t) = 0, \tag{17}$$

$$\nabla\times\mathbf{E}(\mathbf{r},t) = -\frac{d\mathbf{B}(\mathbf{r},t)}{dt}, \tag{18}$$

$$\begin{aligned}\nabla\times\mathbf{B}(\mathbf{r},t) = \mu_0\frac{d}{dt}\big(\epsilon_0\mathbf{E}(\mathbf{r},t) + \mathbf{P}(\mathbf{r},t) - \nabla\cdot\overleftrightarrow{\mathbf{Q}}(\mathbf{r},t)\big)\\ + \mu_0\big(\mathbf{J}_F(\mathbf{r},t) + \nabla\times\mathbf{M}(\mathbf{r},t)\big),\end{aligned} \tag{19}$$

where $\mathbf{E} =< \mathbf{e} >$ and $\mathbf{B} =< \mathbf{b} >$ are the macroscopic electric field and the macroscopic magnetic flux density, respectively. Equations (16)-(19) describe the relations between the macroscopic fields and the macroscopic sources ρ_F, $\mathbf{J}_F$, $\mathbf{P}$, $\mathbf{M}$ and $\overleftrightarrow{\mathbf{Q}}$. Taking the divergence of Eq. (19) and using Eq. (16) yields the continuity equation

$$\frac{d\rho_F(\mathbf{r},t)}{dt} + \nabla\cdot\mathbf{J}_F(\mathbf{r},t) = 0, \tag{20}$$

which allows one to determine ρ_F if $\mathbf{J}_F$ is known.

Let the quantities $\mathbf{E}$, $\mathbf{B}$, $\mathbf{P}$, $\overleftrightarrow{\mathbf{Q}}$, $\mathbf{M}$, ρ_F and $\mathbf{J}_F$ in Eqs. (16)-(19) have a harmonic time variation at an angular frequency ω. In this case we can write the electric field in the form

$$\mathbf{E}(\mathbf{r},t) = \mathrm{Re}\big\{\mathbf{E}(\mathbf{r})e^{-i\omega t}\big\}, \tag{21}$$

which defines the complex amplitude of the electric field, $\mathbf{E}(\mathbf{r})$. Similar equations define the complex amplitudes of $\mathbf{B}$, $\mathbf{P}$, $\overleftrightarrow{\mathbf{Q}}$, $\mathbf{M}$, ρ_F and $\mathbf{J}_F$. For time-harmonic fields the continuity equation in Eq. (20) takes the form

$$i\omega\rho_F(\mathbf{r}) = \nabla\cdot\mathbf{J}_F(\mathbf{r}) \tag{22}$$

that also holds for the complex amplitudes of ρ and $\mathbf{J}$. The Maxwell equations can be written in terms of the introduced complex amplitudes as [19]

$$\nabla\cdot\mathbf{D}(\mathbf{r}) = 0, \tag{23}$$
$$\nabla\cdot\mathbf{B}(\mathbf{r}) = 0, \tag{24}$$
$$\nabla\times\mathbf{E}(\mathbf{r}) = i\omega\mathbf{B}(\mathbf{r}), \tag{25}$$
$$\nabla\times\mathbf{H}(\mathbf{r}) = -i\omega\mathbf{D}(\mathbf{r}), \tag{26}$$

where we have defined the complex amplitude of the electric displacement as

$$\mathbf{D}(\mathbf{r}) = \epsilon_0\mathbf{E}(\mathbf{r}) + \mathbf{P}(\mathbf{r}) - \nabla\cdot\overleftrightarrow{\mathbf{Q}}(\mathbf{r}) + \frac{i}{\omega}\mathbf{J}_F(\mathbf{r}), \tag{27}$$

and the complex amplitude of the magnetic field as

$$\mathbf{H}(\mathbf{r}) = \frac{1}{\mu_0}\mathbf{B}(\mathbf{r}) - \mathbf{M}(\mathbf{r}). \tag{28}$$

In general, the fields are not harmonic in time. However, if the sources $\mathbf{J}_F$, $\mathbf{P}$, $\mathbf{M}$ and $\overleftrightarrow{\mathbf{Q}}$ are linearly related to the fields $\mathbf{E}$ and $\mathbf{B}$, these fields can be written as integrals of $\mathrm{Re}\big\{\mathbf{E}(\mathbf{r})e^{-i\omega t}\big\}$ and $\mathrm{Re}\big\{\mathbf{B}(\mathbf{r})e^{-i\omega t}\big\}$ over ω. Then, Eqs. (23)-(26) may be applied to the integrand for each value of ω separately.

Up to this point we have considered electromagnetic fields in a medium consisting of molecules. The microscopic molecular moments and currents dictate, through Eqs. (11)-(15), the macroscopic properties of the medium. The microscopic properties, which can be rigorously determined by using quantum mechanics, possess restrictions which through averaging transfer onto the macroscopic properties. For example, at optical frequencies we do not find any natural materials where $\mathbf{M}$ would be comparable to $\mathbf{P}$. These restrictions may be overcome by constructing metamaterials.

The idea of metamaterials is to structure matter on a length scale much smaller than the characteristic length of the expected spatial variations of $\mathbf{E}$ and $\mathbf{B}$. This allows one to apply a second spatial averaging, but this time to Eqs. (23)-(26). The structuring can, for example, cause electromagnetic excitation of circulating electric currents, which after averaging appear to result in an effective $\mathbf{M}$ in the new macroscopic Maxwell equations. Constructing metamaterials with significant $\mathbf{M}$ at optical frequencies is of particular interest in the metamaterials research.

2.2 Constitutive relations

In order to solve the macroscopic Maxwell equations one needs to know the sources $\mathbf{J}_F$, $\mathbf{P}$, $\mathbf{M}$ and $\overleftrightarrow{\mathbf{Q}}$. In general, these sources can be complicated functions of the electric field $\mathbf{E}$ and the magnetic flux density $\mathbf{B}$. If this functional dependence is known, we can write $\mathbf{D}$ and $\mathbf{H}$ in Eqs. (27) and (28) as functions of $\mathbf{E}$ and $\mathbf{B}$. These equations, relating $\mathbf{D}$ and $\mathbf{H}$ to $\mathbf{E}$ and $\mathbf{B}$, are called the constitutive relations [17].

As stated before, for natural materials $\overleftrightarrow{\mathbf{Q}}$ can often be neglected. We assume that the medium has no polarization or magnetization in the absence of $\mathbf{E}$ and $\mathbf{B}$. For relatively weak fields, we can assume that $\mathbf{P}$ is linearly proportional to $\mathbf{E}$ and independent of $\mathbf{B}$. Likewise, we assume that $\mathbf{M}$ is linearly proportional to $\mathbf{B}$ and independent of $\mathbf{E}$. Under these assumptions we can write the following general relations [18]

$$\mathbf{P}(\mathbf{r},t) = \epsilon_0 \int \int_{-\infty}^{t} \overleftrightarrow{\chi}_e(\mathbf{r},\mathbf{r}',t,t') \cdot \mathbf{E}(\mathbf{r}',t')dt'd^3r', \tag{29}$$

$$\mathbf{M}(\mathbf{r},t) = \int \int_{-\infty}^{t} \overleftrightarrow{\chi}_m(\mathbf{r},\mathbf{r}',t,t') \cdot \mathbf{B}(\mathbf{r}',t')dt'd^3r', \tag{30}$$

where the dyadics $\overleftrightarrow{\chi}_e$ and $\overleftrightarrow{\chi}_m$ are called the electric and magnetic susceptibilities, as they describe the response of the medium to the electromagnetic fields.

Equations (29) and (30) indicate that $\mathbf{P}$ and $\mathbf{M}$ at an instant of time t may depend on the values of $\mathbf{E}$ and $\mathbf{B}$ at previous instants of times. This effect is called temporal dispersion. Equations (29) and (30) also indicate that $\mathbf{P}$ and $\mathbf{M}$ at a point $\mathbf{r}$ can depend on the values of $\mathbf{E}$ and $\mathbf{B}$ at other points in space, implying non-locality. This effect is called spatial dispersion. Spatial dispersion can usually be neglected for light-matter interaction at optical frequencies by setting $\overleftrightarrow{\chi}_e(\mathbf{r},\mathbf{r}',t,t') = \overleftrightarrow{\chi}_e(\mathbf{r},t,t')\delta(\mathbf{r}-\mathbf{r}')$ and $\overleftrightarrow{\chi}_m(\mathbf{r},\mathbf{r}',t,t') = \overleftrightarrow{\chi}_m(\mathbf{r},t,t')\delta(\mathbf{r}-\mathbf{r}')$.

We assume time-harmonic variation of $\mathbf{E}$ and $\mathbf{B}$. Then Eq. (21) is written for $\mathbf{E}$ and $\mathbf{B}$ and inserted into Eqs. (29) and (30). For time-harmonic fields the response functions only depend on the time difference $t-t'$. Furthermore, the response functions are defined to be zero for $t' > t$, as the material response cannot depend on the future values of $\mathbf{E}$ and $\mathbf{B}$. In terms of the complex amplitudes Eqs. (29) and (30) are in this case written as

$$\mathbf{P}(\mathbf{r}) = \epsilon_0 \overleftrightarrow{\chi}_e(\mathbf{r},\omega) \cdot \mathbf{E}(\mathbf{r}), \tag{31}$$

$$\mathbf{M}(\mathbf{r}) = \overleftrightarrow{\chi}_m(\mathbf{r},\omega) \cdot \mathbf{B}(\mathbf{r}), \tag{32}$$

where

$$\overleftrightarrow{\chi}_e(\mathbf{r},\omega) = \int_{-\infty}^{\infty} \overleftrightarrow{\chi}_e(\mathbf{r},t)e^{i\omega t}dt, \tag{33}$$

$$\overleftrightarrow{\chi}_m(\mathbf{r},\omega) = \int_{-\infty}^{\infty} \overleftrightarrow{\chi}_m(\mathbf{r},t)e^{i\omega t}dt. \tag{34}$$

Similar calculations can be done for the free current density. Assuming that $\mathbf{J}_F$ depends linearly on $\mathbf{E}$, we can derive the Ohm's law

$$\mathbf{J}_F(\mathbf{r}) = \overleftrightarrow{\sigma}(\mathbf{r},\omega)\cdot\mathbf{E}(\mathbf{r}), \tag{35}$$

with $\mathbf{J}_F(\mathbf{r})$ satisfying Eq. (21) and $\overleftrightarrow{\sigma}(\mathbf{r},\omega)$ being the conductivity dyadic of the material. In general, $\overleftrightarrow{\chi}_e(\mathbf{r},\omega)$, $\overleftrightarrow{\chi}_m(\mathbf{r},\omega)$ and $\overleftrightarrow{\sigma}(\mathbf{r},\omega)$ are complex quantities. The presence of the imaginary part means that there is a phase delay between the response of the medium ($\mathbf{P}$, $\mathbf{M}$ or $\mathbf{J}_F$) and the applied field ($\mathbf{E}$ or $\mathbf{B}$). For a propagating electromagnetic wave, this phase delay is physically manifested by absorption of electromagnetic energy.[20]

The electric permittivity dyadic can now be defined as

$$\overleftrightarrow{\epsilon}(\mathbf{r},\omega) = \epsilon_0\overleftrightarrow{\mathbf{I}} + \epsilon_0\overleftrightarrow{\chi}_e(\mathbf{r},\omega) + \frac{i}{\omega}\overleftrightarrow{\sigma}(\mathbf{r},\omega), \tag{36}$$

and the magnetic permeability dyadic as

$$\overleftrightarrow{\mu}(\mathbf{r},\omega) = \Big(\frac{1}{\mu_0}\overleftrightarrow{\mathbf{I}} - \overleftrightarrow{\chi}_m(\mathbf{r},\omega)\Big)^{-1}, \tag{37}$$

where $\overleftrightarrow{\mathbf{I}}$ is the unit dyadic. Usually in textbooks, $\mathbf{M}$ is defined as being proportional to $\mathbf{H}$ which leads to a different $\overleftrightarrow{\chi}_m$ and thus, a different relation in Eq. (37) (see, e.g. [21]). Combining Eqs. (31)-(37) with Eqs. (27) and (28) yields the constitutive relations

$$\mathbf{D}(\mathbf{r}) = \overleftrightarrow{\epsilon}(\mathbf{r},\omega)\cdot\mathbf{E}(\mathbf{r}), \tag{38}$$

$$\mathbf{H}(\mathbf{r}) = \overleftrightarrow{\mu}^{-1}(\mathbf{r},\omega)\cdot\mathbf{B}(\mathbf{r}). \tag{39}$$

For isotropic materials the dyadics $\overleftrightarrow{\epsilon}(\mathbf{r},\omega)$ and $\overleftrightarrow{\mu}(\mathbf{r},\omega)$ are diagonal with all diagonal elements being equal. For these materials we can write $\mathbf{D} = \epsilon_0\epsilon_r\mathbf{E}$ and $\mathbf{B} = \mu_0\mu_r\mathbf{H}$. The complex constants ϵ_r and μ_r are the relative electric permittivity and the relative magnetic permeability, respectively. If in addition the medium is homogeneous, the electric permittivity and magnetic permeability are independent of position $\mathbf{r}$. In this case, the Maxwell equations, Eqs. (23)-(26), reduce to

$$\nabla\cdot\mathbf{E}(\mathbf{r}) = 0, \tag{40}$$

$$\nabla\cdot\mathbf{H}(\mathbf{r}) = 0, \tag{41}$$

$$\nabla\times\mathbf{E}(\mathbf{r}) = ik\eta\mathbf{H}(\mathbf{r}), \tag{42}$$

$$\nabla\times\mathbf{H}(\mathbf{r}) = -\frac{ik}{\eta}\mathbf{E}(\mathbf{r}), \tag{43}$$

where we have introduced the wave number in the medium

$$k = \frac{\omega}{c}\sqrt{\mu_r\epsilon_r}, \tag{44}$$

and impedance

$$\eta = \sqrt{\frac{\mu_0\mu_r}{\epsilon_0\epsilon_r}}. \tag{45}$$

A frequently used solution to Eqs. (40)-(43) is the electromagnetic plane wave, the complex amplitude of which has the form

$$\mathbf{E}(\mathbf{r}) = \mathbf{E}_0 e^{i\mathbf{k}\cdot\mathbf{r}}, \tag{46}$$

where $\mathbf{E}_0$ is a constant and the wave vector $\mathbf{k}$ points in the direction of the wave propagation. The magnitude of $\mathbf{k}$ is given by Eq. (44). The periodicity of the plane wave in the $\mathbf{k}$ direction defines the wavelength $\lambda = 2\pi/k$. The magnetic field of the plane wave can be calculated using Eq. (42).

In the case of metamaterials, one can perform a second spatial averaging and obtain Eqs. (23)-(26) with $\mathbf{J}_F$, $\mathbf{P}$, $\mathbf{M}$ and $\overleftrightarrow{\mathbf{Q}}$ determined by both the material properties and the shapes of the meta-atoms. For optical metamaterials neglect of $\overleftrightarrow{\mathbf{Q}}$ is not justified [15, 22]. In particular, in Sec. 3.2 we show that time-harmonic magnetic dipole and electric quadrupole moments of meta-atoms are produced by similar electric current excitations. It would then be of interest to derive the effective parameters similar to those in Eqs. (36)-(37) which would describe the electromagnetic properties of the homogenized metamaterial. Especially, by constructing an isotropic metamaterial with negative μ_r and ϵ_r, one can obtain a medium exhibiting negative refraction [5, 6].

At optical frequencies, the constituent materials used to create a metamaterial are not magnetic. Therefore it is the electric field, and not the magnetic flux density, that induces the effective magnetization $\mathbf{M}$ [23, 24]. One also has to note that optical meta-atoms typically have dimensions on the order of 10 nm. The averaging volume used to homogenize the metamaterial would then have a linear dimension of at least several tens of nanometers. The visible light wavelength is not much larger than the size of the averaging volume. As a consequence, the spatial dispersion in Eqs. (29) and (30) can no longer be neglected. The spatial dispersion manifests itself in $\mathbf{D}$ being dependent on the spatial gradients of $\mathbf{E}$. In general, this causes the obtained permittivity dyadic to depend on the orientation of the wave vector $\mathbf{k}$ [18]. Only if the spatial dispersion of the metamaterial is weak, effective material parameters that do not depend on $\mathbf{k}$ can be introduced [25].

2.3 Boundary conditions

A common situation in the macroscopic field-matter interaction is that the properties of a medium in question change abruptly across the medium's boundaries. One can then solve the Maxwell equations separately in each region of space in which the medium is homogeneous. The solutions will contain unknown parameters. Boundary conditions connect these solutions and allow one to find the values of the unknown parameters.

In standard textbook derivations of the boundary conditions, the quadrupole moment density $\overleftrightarrow{\mathbf{Q}}$, being considered to be small, is ignored [17]. However, this cannot be done when dealing with metamaterials. The boundary conditions at an interface between vacuum and a dielectric with non-negligible quadrupole moment density have been obtained previously [2]. Even though the calculation was done for

a homogeneous dielectric, it is equally applicable to a homogenized metamaterial.

In the derivation of Ref. [2] the following geometry is considered. A time-harmonic plane wave (see Eq. (46)) is incident from vacuum onto a semi-infinite homogeneous dielectric. The dielectric fills the $z > 0$ half-space. The free current density in the dielectric is set to zero. Furthermore, a dynamic permittivity dyadic $\overleftrightarrow{\upsilon}$ describing the dielectric is defined such that Eq. (10) can be written in the form

$$\mathbf{J}(\mathbf{r}) = -i\omega\big(\overleftrightarrow{\upsilon}(\mathbf{k},\omega) - \epsilon_0\overleftrightarrow{\mathbf{I}}\big)\cdot\mathbf{E}(\mathbf{r}). \tag{47}$$

The dynamic permittivity dyadic contains all information about the medium, including its magnetic properties. In general, the dyadic can depend on the propagation direction of the plane wave. This is a consequence of spatial derivatives in Eq. (10). For materials with $\mathbf{M} = 0$ and $\overleftrightarrow{\mathbf{Q}} = 0$, it follows that $\overleftrightarrow{\upsilon} = \overleftrightarrow{\epsilon}$.

We denote the fields in vacuum with a subscript 1, whereas the fields in the dielectric are denoted with a subscript 2. The boundary conditions that establish the relation between the various projections of the fields at $z = 0$ are [2]

$$E_{2x} - E_{1x} = \frac{d}{dx}\frac{Q_{zz}}{\upsilon_{zz}}, \tag{48}$$

$$E_{2y} - E_{1y} = \frac{d}{dy}\frac{Q_{zz}}{\upsilon_{zz}}, \tag{49}$$

$$D_{2z} - D_{1z} = \frac{d}{dx}\big(Q_{xz} - \upsilon_{xz}\frac{Q_{zz}}{\upsilon_{zz}}\big) + \frac{d}{dy}\big(Q_{yz} - \upsilon_{yz}\frac{Q_{zz}}{\upsilon_{zz}}\big), \tag{50}$$

$$H_{2x} - H_{1x} = i\omega Q_{yz} - i\omega\upsilon_{yz}\frac{Q_{zz}}{\upsilon_{zz}}, \tag{51}$$

$$H_{2y} - H_{1y} = -i\omega Q_{xz} + i\omega\upsilon_{xz}\frac{Q_{zz}}{\upsilon_{zz}}, \tag{52}$$

$$B_{2z} - B_{1z} = 0. \tag{53}$$

In Eqs. (48)-(53), $\mathbf{D}$ and $\mathbf{H}$, as defined by Eqs. (38) and (39), are used. If the dielectric has negligible quadrupole moment density, Eqs. (48)-(53) become the ordinary textbook boundary conditions [17]. The vector projections of $\mathbf{E}$ and $\mathbf{H}$ onto the interface are then equal on both sides of the boundary. However, in the presence of quadrupole moments we have to use the expressions in Eqs. (48)-(53). It is interesting that in this case, the tangential components E_x and E_y are not necessarily continuous across the interface, which is related to the fact that the quadrupole moment density creates a surface density of the bound electric dipole moment that can spatially vary along the surface [3]. The surface density of the bound electric dipole moment is present only in magnetic media [3]. In the usual derivations of boundary conditions it is assumed that the interface can introduce only a surface density of electric charge, and all higher order surface moments are neglected. Thus, the ordinary boundary conditions result from the dipole approximation of the molecules.

2.4 The multipole expansion

Next we search for a general solution of Eqs. (40)-(43) that can be used to describe the fields generated by a meta-atom. We restrict the solution to such media in which ϵ_r and μ_r are positive real numbers. Taking the curl of Eqs. (42) and (43) yields the following Helmholtz equations

$$(\nabla^2 + k^2)\mathbf{E}(\mathbf{r}) = 0, \tag{54}$$
$$(\nabla^2 + k^2)\mathbf{H}(\mathbf{r}) = 0. \tag{55}$$

For the divergenceless fields (see Eqs. (40) and (41)), the general solution to Eqs. (54) and (55) can be written in spherical coordinates as [17]

$$\mathbf{H}(\mathbf{r}) = \sum_{l=1}^{\infty}\sum_{m=-l}^{l}\Big(a_E(l,m)f_l(kr)\mathbf{X}_{lm} - \frac{i}{k}a_M(l,m)\nabla\times\big(g_l(kr)\mathbf{X}_{lm}\big)\Big), \tag{56}$$

$$\mathbf{E}(\mathbf{r}) = \eta\sum_{l=1}^{\infty}\sum_{m=-l}^{l}\Big(\frac{i}{k}a_E(l,m)\nabla\times\big(f_l(kr)\mathbf{X}_{lm}\big) + a_M(l,m)g_l(kr)\mathbf{X}_{lm}\Big), \tag{57}$$

where

$$\mathbf{X}_{lm}(\theta,\phi) = \frac{-i}{\sqrt{l(l+1)}}(\mathbf{r}\times\nabla)Y_{lm}(\theta,\phi), \tag{58}$$

and

$$Y_{lm}(\theta,\phi) = \sqrt{\frac{2l+1}{4\pi}\frac{(l-m)!}{(l+m)!}}P_l^m(\cos\theta)e^{im\phi}. \tag{59}$$

The angular functions $\mathbf{X}_{lm}$ are the vector spherical harmonics and Y_{lm} are the scalar spherical harmonics. The functions P_l^m are the associated Legendre polynomials of degree l and order m, defined through the Rodrigues' formula

$$P_l^m(\cos\theta) = \frac{(-1)^m}{2^l l!}(\sin\theta)^m\frac{d^{l+m}}{d(\cos\theta)^{l+m}}\big((\cos\theta)^2-1\big)^l. \tag{60}$$

Note that in some literature, e.g. in Ref. [21], the associated Legendre polynomials are defined without the factor $(-1)^m$. The radial functions in Eqs. (56) and (57) are

$$f_l(kr) = A_l^{(1)}h_l^{(1)}(kr) + A_l^{(2)}h_l^{(2)}(kr), \tag{61}$$
$$g_l(kr) = B_l^{(1)}h_l^{(1)}(kr) + B_l^{(2)}h_l^{(2)}(kr), \tag{62}$$

where $h_l^{(1)}$ and $h_l^{(2)}$ are the spherical Hankel functions of the first and second kind, respectively, of order l [17]. The values of the expansion coefficients $a_E(l,m)$, $a_M(l,m)$, $A_l^{(1)}$, $A_l^{(2)}$, $B_l^{(1)}$ and $B_l^{(2)}$ determine the electric and magnetic fields.

In Eqs. (56) and (57), the coefficients $a_E(l,m)$ describe electric multipole radiation, whereas $a_M(l,m)$ describe magnetic multipole radiation. The electric monopole coefficient $a_E(0,0)$ has been neglected as we are ultimately interested in phenomena in which the fields are generated by localized sources. Each localized source is considered to be electrically neutral, implying that it cannot have a harmonically os-

cillating net charge (see also Eq. (40)). The magnetic monopole coefficient $a_M(0,0)$ is also equal to zero.

We assume that the electromagnetic fields are generated by localized sources, e.g., by an optically excited dielectric or metal particle. We consider a small imaginary sphere of radius R that encloses all these sources. The fields outside the sphere can then be expanded through Eqs. (56) and (57), with the coordinate system origin chosen somewhere inside the sphere. The fields outside the sphere must decay with increasing distance from the origin. The spherical Hankel functions of the second kind do not decay with increasing argument. Thus, we must choose $A_l^{(2)} = B_l^{(2)} = 0$ in the expansion. The remaining coefficients $A_l^{(1)}$ and $B_l^{(1)}$ are then scaling factors for the coefficients $a_E(l,m)$ and $a_M(l,m)$ and can therefore be chosen arbitrarily. We choose the scaling factors to be such, that the quantities derived from the multipole expansion assume neat looking expressions.

We define our multipole expansion as

$$\begin{aligned}\mathbf{E}(r,\theta,\phi) =& E_0 \sum_{l=1}^{\infty} \sum_{m=-l}^{l} i^l \sqrt{\pi(2l+1)} \\ & \left(\frac{1}{k} a_E(l,m) \nabla \times \left(h_l^{(1)}(kr)\mathbf{X}_{lm}\right) + a_M(l,m) h_l^{(1)}(kr)\mathbf{X}_{lm}\right), \qquad (63)\\ \mathbf{H}(r,\theta,\phi) =& \frac{E_0}{\eta} \sum_{l=1}^{\infty} \sum_{m=-l}^{l} i^{l-1} \sqrt{\pi(2l+1)} \\ & \left(\frac{1}{k} a_M(l,m) \nabla \times \left(h_l^{(1)}(kr)\mathbf{X}_{lm}\right) + a_E(l,m) h_l^{(1)}(kr)\mathbf{X}_{lm}\right), \qquad (64)\end{aligned}$$

where E_0 is an electric field amplitude factor. The relation between E_0 and the sources is defined in Sec. 3.1. The multipole expansion is useful, if the sphere enclosing the sources has a radius which is small compared to the wavelength. This implies that kR is small and ensures that only the first few l terms are significant in the expansion. A mapping between the types of sources and the radiated fields of certain orders of l and m is given in Sec. 3.2.

The vector spherical harmonics form an orthogonal set of functions, for which we have

$$\int \mathbf{X}^*_{l'm'}(\theta,\phi) \cdot \mathbf{X}_{lm}(\theta,\phi) d\Omega = \delta_{ll'}\delta_{mm'}. \qquad (65)$$

This is a consequence of the orthogonality of the spherical harmonics:

$$\int Y^*_{l'm'}(\theta,\phi) Y_{lm}(\theta,\phi) d\Omega = \delta_{ll'}\delta_{mm'}. \qquad (66)$$

Furthermore, the electric and magnetic multipole radiations in Eqs. (63) and (64) are orthogonal to each other. Owing to the above orthogonalities, the multipole coefficients $a_E(l,m)$ and $a_M(l,m)$ are uniquely defined for each electromagnetic field.[17]

It is useful to write Eqs. (63) and (64) in a component form. We first define the following functions

$$O_{lm} = \frac{1}{\sqrt{l(l+1)}}\sqrt{\frac{2l+1}{4\pi}\frac{(l-m)!}{(l+m)!}}, \tag{67}$$

$$\tau_{lm}(\theta) = \frac{d}{d\theta}P_l^m(\cos\theta), \tag{68}$$

$$\pi_{lm}(\theta) = \frac{m}{\sin\theta}P_l^m(\cos\theta), \tag{69}$$

$$\xi_l(kr) = krh_l^{(1)}(kr). \tag{70}$$

The definition of $\mathbf{X}_{lm}$ together with recursion formulas for the associated Legendre polynomials (see Appendix A.1) yield the electric field components

$$E_r(r,\theta,\phi) = \frac{E_0}{(kr)^2}\sum_{l=1}^{\infty}\sum_{m=-l}^{l}\sqrt{\pi(2l+1)}i^{l+1}l(l+1)O_{lm} a_E(l,m)\xi_l(kr)P_l^m(\cos\theta)e^{im\phi}, \tag{71}$$

$$E_\theta(r,\theta,\phi) = \frac{E_0}{kr}\sum_{l=1}^{\infty}\sum_{m=-l}^{l}\sqrt{\pi(2l+1)}i^{l}O_{lm} \Big(ia_E(l,m)\xi_l'(kr)\tau_{lm}(\theta) - a_M(l,m)\xi_l(kr)\pi_{lm}(\theta)\Big)e^{im\phi}, \tag{72}$$

$$E_\phi(r,\theta,\phi) = \frac{E_0}{kr}\sum_{l=1}^{\infty}\sum_{m=-l}^{l}\sqrt{\pi(2l+1)}i^{l}O_{lm} \Big(-a_E(l,m)\xi_l'(kr)\pi_{lm}(\theta) - ia_M(l,m)\xi_l(kr)\tau_{lm}(\theta)\Big)e^{im\phi}. \tag{73}$$

The superscript in ξ_l' means differentiation with respect to the argument, kr. We notice that Eqs. (63) and (64) are symmetric with respect to the interchange $[\mathbf{E}, a_E(l,m), a_M(l,m)] \leftrightarrow [i\eta\mathbf{H}, a_M(l,m), a_E(l,m)]$. This allows us to directly deduce the magnetic field components

$$H_r(r,\theta,\phi) = \frac{E_0}{\eta(kr)^2}\sum_{l=1}^{\infty}\sum_{m=-l}^{l}\sqrt{\pi(2l+1)}i^{l}l(l+1)O_{lm} a_M(l,m)\xi_l(kr)P_l^m(\cos\theta)e^{im\phi}, \tag{74}$$

$$H_\theta(r,\theta,\phi) = \frac{E_0}{\eta kr}\sum_{l=1}^{\infty}\sum_{m=-l}^{l}\sqrt{\pi(2l+1)}i^{l}O_{lm} \Big(a_M(l,m)\xi_l'(kr)\tau_{lm}(\theta) + ia_E(l,m)\xi_l(kr)\pi_{lm}(\theta)\Big)e^{im\phi}, \tag{75}$$

$$H_\phi(r,\theta,\phi) = \frac{E_0}{\eta kr}\sum_{l=1}^{\infty}\sum_{m=-l}^{l}\sqrt{\pi(2l+1)}i^{l}O_{lm} \Big(ia_M(l,m)\xi_l'(kr)\pi_{lm}(\theta) - a_E(l,m)\xi_l(kr)\tau_{lm}(\theta)\Big)e^{im\phi}. \tag{76}$$

We now consider a situation where we know the complex fields $\mathbf{E}(\mathbf{r})$ and $\mathbf{H}(\mathbf{r})$ outside a localized source. Then we can always write the fields as a multipole expansion in the form of Eqs. (63) and (64). The orthogonality of the vector spherical

harmonics in Eq. (65) allows us to determine the multipole coefficients through

$$a_E(l,m) = \frac{\eta}{E_0 i^{l-1}\sqrt{\pi(2l+1)}h_l^{(1)}(kr)} \int \mathbf{X}_{lm}^* \cdot \mathbf{H}(\mathbf{r}) d\Omega, \tag{77}$$

$$a_M(l,m) = \frac{1}{E_0 i^{l}\sqrt{\pi(2l+1)}h_l^{(1)}(kr)} \int \mathbf{X}_{lm}^* \cdot \mathbf{E}(\mathbf{r}) d\Omega, \tag{78}$$

where the integration is performed over any spherical surface of radius r enclosing the sources. The vector spherical harmonics have no radial components. Thus, Eqs. (77) and (78) state that the knowledge of the θ- and ϕ-components of $\mathbf{E}$ and $\mathbf{H}$ on any spherical surface enclosing the sources is enough to determine the multipole coefficients.

The multipole coefficients can also be obtained from the radial components of $\mathbf{E}$ and $\mathbf{H}$. The orthogonality of the spherical harmonics in Eq. (66) allows us to determine the multipole coefficients from Eqs. (71) and (74) as

$$a_E(l,m) = \frac{kr}{E_0 i^{l+1}\sqrt{\pi(2l+1)}\sqrt{l(l+1)}h_l^{(1)}(kr)} \int Y_{lm}^* E_r(\mathbf{r}) d\Omega, \tag{79}$$

$$a_M(l,m) = \frac{\eta kr}{E_0 i^{l}\sqrt{\pi(2l+1)}\sqrt{l(l+1)}h_l^{(1)}(kr)} \int Y_{lm}^* H_r(\mathbf{r}) d\Omega. \tag{80}$$

Equations (79) and (80) state that the knowledge of the radial components of $\mathbf{E}$ and $\mathbf{H}$ on any spherical surface enclosing the sources is enough to determine the multipole coefficients. The choice of which combination of Eqs. (77)-(80) to use, is a matter of preference. For example, if one only wants to deal with $\mathbf{E}$, one can choose to use Eqs. (78) and (79) to obtain the multipole coefficients.

It is also possible to deduce the multipole coefficients directly from the distribution of electric current in the source. For simplicity, we assume that $\mathbf{M} = 0$ everywhere, such that Eq. (27) is $\mathbf{D} = \epsilon_0\mathbf{E} + i\mathbf{J}/\omega$. Unless the surrounding medium is vacuum, $\mathbf{J}$ is not localized due to polarization currents. We therefore define a source current density $\mathbf{J}_S$, such that

$$\mathbf{D}(\mathbf{r}) = \epsilon_0\epsilon_r\mathbf{E}(\mathbf{r}) + \frac{i}{\omega}\mathbf{J}_S(\mathbf{r}), \tag{81}$$

where ϵ_r has a fixed value equal to the relative electric permittivity of the surrounding medium. The source current density $\mathbf{J}_S$ is zero outside the source. Only if the surrounding medium is vacuum, $\mathbf{J}_S = \mathbf{J}$. In Sec. 3.1, we relate $\mathbf{J}_S$ to the electric field in a light scattering problem. Using Eq. (81), we can write Coulomb's law and the Ampère-Maxwell law in Eqs. (23) and (26) as

$$\nabla \cdot \mathbf{E}(\mathbf{r}) = -\frac{i\eta}{k}\nabla \cdot \mathbf{J}_S(\mathbf{r}), \tag{82}$$

$$\nabla \times \mathbf{H}(\mathbf{r}) = -\frac{ik}{\eta}\mathbf{E}(\mathbf{r}) + \mathbf{J}_S(\mathbf{r}), \tag{83}$$

which converge to Eqs. (40) and (43) if $\mathbf{J}_S = 0$. This ensures that outside the sources the multipole expansion stays valid. Note that in Eqs. (82) and (83), k and η refer to the values in the surrounding medium.

Taking the curl of Eqs. (42) and (83) enables derivation of the wave equations [17]. Using the vector identity $[\mathbf{r}\cdot(\nabla^2\mathbf{E}) = \nabla^2(\mathbf{r}\cdot\mathbf{E}) - 2\nabla\cdot\mathbf{E}]$ one can derive the radial wave equations

$$\big(\nabla^2 + k^2\big)\big(\mathbf{r}\cdot\mathbf{E}(\mathbf{r})\big) = -ik\eta\mathbf{r}\cdot\mathbf{J}_S(\mathbf{r}) - i\frac{\eta}{k}\big(2 + r\frac{d}{dr}\big)\big(\nabla\cdot\mathbf{J}_S(\mathbf{r})\big), \tag{84}$$

$$\big(\nabla^2 + k^2\big)\big(\mathbf{r}\cdot\mathbf{H}(\mathbf{r})\big) = -\mathbf{r}\cdot\big(\nabla\times\mathbf{J}_S(\mathbf{r})\big). \tag{85}$$

Outside the sources, the solution to these are given by the volume integrals [17]

$$rE_r(\mathbf{r}) = \frac{i\eta}{k}\int\frac{e^{ik|\mathbf{r}-\mathbf{r}'|}}{4\pi|\mathbf{r}-\mathbf{r}'|}\Big(k^2\mathbf{r}'\cdot\mathbf{J}_S(\mathbf{r}') + \big(2 + r'\frac{d}{dr'}\big)\big(\nabla'\cdot\mathbf{J}_S(\mathbf{r}')\big)\Big)d^3r', \tag{86}$$

$$rH_r(\mathbf{r}) = \int\frac{e^{ik|\mathbf{r}-\mathbf{r}'|}}{4\pi|\mathbf{r}-\mathbf{r}'|}\mathbf{r}'\cdot\big(\nabla'\times\mathbf{J}_S(\mathbf{r}')\big)d^3r'. \tag{87}$$

The multipole coefficients can be obtained by inserting Eqs. (86) and (87) into Eqs. (79) and (80). One then needs the spherical wave projections [17]

$$\int\frac{e^{ik|\mathbf{r}-\mathbf{r}'|}}{4\pi|\mathbf{r}-\mathbf{r}'|}Y^*_{lm}(\theta,\phi)d\Omega = ikh^{(1)}_l(kr)j_l(kr')Y^*_{lm}(\theta',\phi'), \tag{88}$$

where j_l is the spherical Bessel function. After performing consecutive steps of partial integration to get rid of all spatial derivatives of $\mathbf{J}_S$, we obtain

$$\begin{aligned} a_E(l,m) =& \frac{k^2\eta}{i^{l-1}E_0\sqrt{\pi(2l+1)}}O_{lm}\int e^{-im\phi}\Big(J_{Sr}(\mathbf{r})P^m_l(\cos\theta)\big(\Psi_l(kr) + \Psi''_l(kr)\big) \\ &+ \frac{\Psi'_l(kr)}{kr}\big(\tau_{lm}(\theta)J_{S\theta}(\mathbf{r}) - i\pi_{lm}(\theta)J_{S\phi}(\mathbf{r})\big)\Big)d^3r, \end{aligned} \tag{89}$$

$$\begin{aligned} a_M(l,m) =& \frac{k^2\eta}{i^{l+1}E_0\sqrt{\pi(2l+1)}}O_{lm}\int e^{-im\phi}j_l(kr)\big(iJ_{S\theta}(\mathbf{r})\pi_{lm}(\theta) \\ &+ J_{s\phi}(\mathbf{r})\tau_{lm}(\theta)\big)d^3r, \end{aligned} \tag{90}$$

which gives the multipole coefficients in terms of volume integrals of the source current density vector components J_{Sr}, $J_{S\theta}$ and $J_{S\phi}$. The Riccati-Bessel functions Ψ_l in Eqs. (89) and (90) are described in A.3. If the source current density distribution is known, numerically or otherwise, Eqs. (89) and (90) enable calculation of the multipole coefficients.

We have now derived three ways to calculate the multipole coefficients describing the radiation from a localized source. One can either use angular integrals over the radial fields, angular integrals over the angular fields or volume integrals over the source current density distribution. The first two approaches are not applicable to a situation where the fields generated by the source of interest cannot be separated from the fields generated by other, surrounding, sources. For example, for an infinite array of localized sources, the fields at each point in space are superpositions of the radiation from each individual source. Since the superposition contains incoming waves from adjacent sources, the total field cannot be expanded with an expansion in which $h^{(2)}_l$ are neglected.

In contrast, Eqs. (89) and (90) can be applied also to situations where we have infinite arrays of sources. By integrating the current density distribution of a single source we obtain a multipole expansion describing this single source. The expansion is meaningful assuming that the current density distribution is obtained in a way where the influence of the adjacent sources has been properly taken into account. The multipole expansion then gives only the contribution of this single source to the total field.

3 Multipole excitations in meta-atoms

In this section, we analyze the excitation of multipole moments in meta-atoms by light. In Sec. 3.1, we apply the multipole expansion, which we have introduced in the previous section, to the problem of light scattering by small structures. In Sec. 3.2, we introduce the concept of point multipoles of electric current and relate these currents to the multipole expansion. The obtained relations provide us with a deeper understanding of the connection between the electric and magnetic properties of meta-atoms. Individual meta-atoms can incorporate more than one nanoparticle. Thus, in Sec. 3.3 we use a quasistatic dipole-dipole interaction model to study the electric current excitations in a nanoparticle dimer. Finally, in Sec. 3.4 we rigorously prove, that the radiation from a metadimer consisting of two electric dipoles has both electric quadrupole and magnetic dipole character.

3.1 Application of the multipole expansion to light scattering

In Sec. 2.1, it was explained how the microscopic properties of molecules determine the macroscopic properties of matter. It was also mentioned that, through structuring of matter on a sub-wavelength scale, we can construct metamaterials with significantly altered electromagnetic properties. In order to study how these properties can be adjusted by the structuring, one needs to develop an appropriate electromagnetic model for the metamaterials. In this subsection we apply our multipole expansion to analyze certain optical metallo-dielectric metamaterials.

We consider structures where efficient nano-scale scatterers, such as metal nanoparticles, are embedded into an otherwise homogeneous and isotropic dielectric. A light wave propagating in the dielectric induces an electric polarization $\mathbf{P}$ in the particle material. Because the particles are made of a different material than the surrounding dielectric, $\mathbf{P}$ is discontinuous across the particle boundaries. This discontinuity generates bound surface charges. If the particle is metallic, the light wave also induces a free current density $\mathbf{J}_F$ within the particle. The oscillating currents and bound charges radiate electromagnetic energy in various directions. This radiation is called scattered radiation [20], and the particles are called scatterers. The light scattered by the particles superposes onto the incident light wave, resulting in a modified wave propagation. In natural materials, it is the light scattered by atoms and molecules that modifies the electromagnetic fields in a way specific for each particular material. Similarly, in metamaterials it is the light scattered by the artificial scatterers that modifies the electromagnetic fields in the material. Because of this analogy, we address the individual scatterers as meta-atoms.

Let us consider light scattering by an individual meta-atom. The constituent materials of the metamaterial are assumed to be linear, which means that we can analyze time-harmonic fields without any loss of generality. At optical frequencies we can set $\mu_r = 1$ everywhere. The surrounding dielectric is assumed to have a positive real-valued ϵ_r. We can then split the electromagnetic field into two parts -

the fields of the incident light, $\mathbf{E}_i$ and $\mathbf{H}_i$, and the fields of the scattered light, $\mathbf{E}_s$ and $\mathbf{H}_s$, - as

$$\mathbf{E}(\mathbf{r}) = \mathbf{E}_i(\mathbf{r}) + \mathbf{E}_s(\mathbf{r}), \tag{91}$$

$$\mathbf{H}(\mathbf{r}) = \mathbf{H}_i(\mathbf{r}) + \mathbf{H}_s(\mathbf{r}). \tag{92}$$

In the dielectric, both the incident and scattered fields satisfy the Maxwell equations given in Eqs. (40)-(43). Outside a smallest sphere that can enclose the meta-atom, the scattered fields may be expanded with our multipole expansion in Eqs. (63) and (64). The multipole expansion forms a complete orthogonal basis which can be used to expand any electromagnetic field generated by a single meta-atom.

If the incident fields are known, the electromagnetic boundary conditions can be used to calculate the scattered fields. Except for meta-atoms of very simple shapes, such as spheres, numerical techniques are required to calculate the scattered field. Once the scattered fields have been obtained, Eqs. (77)-(80) can be used to obtain the multipole expansion coefficients. Alternatively, we can use Eqs. (89) and (90). We note, however, that unless the surrounding dielectric is vacuum, the source current density $\mathbf{J}_S$ in Eqs. (89) and (90) is not the macroscopic current density in the scatterer. Instead, if the scatterer is made of an isotropic material, we can use Eqs. (38) and (81) to obtain

$$\mathbf{J}_S(\mathbf{r}) = -i\omega\epsilon_0\Big(\epsilon_r(\mathbf{r}) - \epsilon_{r,d}\Big)\mathbf{E}(\mathbf{r}), \tag{93}$$

where $\epsilon_{r,d}$ is the positive real-valued relative electric permittivity of the dielectric and $\epsilon_r(\mathbf{r})$ the complex-valued relative electric permittivity at any coordinate of interest. The source current density is the source of the scattered field $\mathbf{E}_s$. Notice that the total field $\mathbf{E}$ is used in Eq. (93). According to Eq. (93), a deviation in the permittivity from that of the surrounding medium is required for the scattering to take place.

At visible light frequencies, particles made of noble metals have remarkably high scattering efficiencies owing to resonant excitations of the conduction electrons in the metal. At the metal surface, the surface charge oscillations are coupled resonantly to the incident electromagnetic field, which enhances the scattering. These coupled surface charge oscillations are commonly referred to as surface plasmon polaritons [26]. The frequency and strength of the resonance depends strongly on the shape of the particles. Due to the high scattering efficiency and tunability of the plasmon resonance frequency, metal scatterers are widely used to create meta-atoms.

When a light wave interacts with a scatterer, the electromagnetic energy is transferred from the incident wave to the scattered wave. In the following, we derive an expression describing this energy transfer as a function of the multipole coefficients. The derivation is analogous to what has been done for the light scattering by a sphere [20].

A plane wave, as given by Eq. (46), is incident upon a scatterer. The scattered fields are expanded using the multipole expansion in Eqs. (63) and (64), where the constant E_0 is the amplitude of the incident plane wave. The scatterer can be surrounded by some imaginary sphere of radius r, centered at the origin of the coordinate system. The scattered light causes a flow of electromagnetic energy

through the surface of this sphere. The time-averaged energy flow rate is

$$W_s = \int \hat{\mathbf{r}} \cdot \mathbf{S}_s(r,\theta,\phi) r^2 d\Omega, \tag{94}$$

where the integration is taken over the entire solid angle and the time-averaged Poynting vector of the scattered radiation is

$$\mathbf{S}_s(\mathbf{r}) = \frac{1}{2}\mathrm{Re}\big\{\mathbf{E}_s(\mathbf{r}) \times \mathbf{H}_s^*(\mathbf{r})\big\}. \tag{95}$$

The integral in Eq. (94) is calculated for the fields $\mathbf{E}_s$ and $\mathbf{H}_s$ expanded as in Eqs. (63) and (64). The integration is done by first using the orthogonality relation of $e^{im\phi}$ and then the orthogonality relations of the τ_{lm} and π_{lm} functions (see Appendix A.2). Equation (A24) together with the Re{} operator in Eq. (95) appear to remove the dependence of W_s on r. The energy flow rate in Eq. (94) becomes

$$W_s = \frac{\pi |E_0|^2}{2\eta k^2} \sum_{l=1}^{\infty} \sum_{m=-l}^{l} (2l+1)\big(|a_E(l,m)|^2 + |a_M(l,m)|^2\big). \tag{96}$$

The time-averaged Poynting vector of the incident plane wave is

$$\mathbf{S}_i(\mathbf{r}) = \frac{1}{2}\mathrm{Re}\big\{\mathbf{E}_i(\mathbf{r}) \times \mathbf{H}_i^*(\mathbf{r})\big\}. \tag{97}$$

The intensity of a plane wave is equal to the magnitude of the time-averaged Poynting vector. Inserting the electric field of Eq. (46) and the corresponding magnetic field into Eq. (97) yields the intensity

$$I_0 = \frac{|E_0|^2}{2\eta}. \tag{98}$$

Dividing the energy flow rate in Eq. (96) with the incident intensity in Eq. (98) defines the scattering cross section

$$C_s = \frac{\pi}{k^2} \sum_{l=1}^{\infty} \sum_{m=-l}^{l} (2l+1)\big(|a_E(l,m)|^2 + |a_M(l,m)|^2\big). \tag{99}$$

The scattering cross section can be interpreted as the area, from which the scatterer takes energy off from the incident plane wave and converts it into scattered light.

There can also be absorption of the electromagnetic energy inside the scatterer. A non-zero imaginary part of ϵ_r implies the presence of the absorption. Especially metal particles absorb well at visible frequencies. In the following, we derive an expression describing the absorption as a function of the multipole coefficients.

The time-averaged Poynting vector

$$\mathbf{S}(\mathbf{r}) = \frac{1}{2}\mathrm{Re}\big\{\mathbf{E}(\mathbf{r}) \times \mathbf{H}^*(\mathbf{r})\big\}, \tag{100}$$

where $\mathbf{E}$ and $\mathbf{H}$ are given by Eqs. (91) and (92), includes the contributions from both the incident and scattered fields. The power absorbed by the scatterer equals the

net rate of electromagnetic energy flowing into the sphere enclosing the scatterer:

$$W_a = -\int \hat{\mathbf{r}} \cdot \mathbf{S}(r,\theta,\phi) r^2 d\Omega. \tag{101}$$

Equations (91) and (92) can be inserted into Eq. (100) to obtain

$$\mathbf{S}(\mathbf{r}) = \mathbf{S}_i(\mathbf{r}) + \mathbf{S}_s(\mathbf{r}) + \mathbf{S}_{int}(\mathbf{r}), \tag{102}$$

where the interference term is

$$\mathbf{S}_{int}(\mathbf{r}) = \frac{1}{2}\mathrm{Re}\big\{\mathbf{E}_i(\mathbf{r}) \times \mathbf{H}_s^*(\mathbf{r}) + \mathbf{E}_s(\mathbf{r}) \times \mathbf{H}_i^*(\mathbf{r})\big\}. \tag{103}$$

Using Eq. (102) in Eq. (101) results in three integrals. The first integral describes the attenuation of the incident field in the absence of the scatterer. Because the surrounding medium does not absorb energy, we have

$$\int \hat{\mathbf{r}} \cdot \mathbf{S}_i(r,\theta,\phi) r^2 d\Omega = 0. \tag{104}$$

The second integral is the previously calculated flow rate of the scattered energy, given in Eq. (94). The third integral,

$$W_{ext} = -\int \hat{\mathbf{r}} \cdot \mathbf{S}_{int}(r,\theta,\phi) r^2 d\Omega, \tag{105}$$

we call the energy extinction rate. Combining Eqs. (94), (101) and (105) yields

$$W_{ext} = W_a + W_s, \tag{106}$$

which explains the choice of the word "extinction". The energy extinction rate describes the rate at which energy is removed from the incident light mode due to both scattering and absorption. Thus, we first calculate W_{ext} and then use Eq. (106) to obtain W_a.

In order to calculate W_{ext} we must specify the polarization of the incident light. We consider the incident light to be linearly x-polarized and to propagate in the $\hat{\mathbf{z}}$ direction, such that

$$\mathbf{E}_i(\mathbf{r}) = \hat{\mathbf{x}} E_0 e^{ikz}. \tag{107}$$

We also need to perform the multipole expansion on this plane wave. This has been done in Ref. [17] for a circularly polarized plane wave. An x-polarized wave can be seen as a superposition of two waves with right- and left-handed circular polarizations. Thus, Eq. (107) can be expanded as

$$\mathbf{E}_i(\mathbf{r}) = \frac{E_0}{2}\sum_{l=1}^{\infty}\sum_{m=-1,+1} i^l \sqrt{4\pi(2l+1)}\Big(j_l(kr)\mathbf{X}_{lm} + \frac{m}{k}\nabla \times \big(j_l(kr)\mathbf{X}_{lm}\big)\Big). \tag{108}$$

The magnetic field $\mathbf{H}_i$ is obtained by inserting $\mathbf{E}_i$ into the Faraday's law, Eq. (42), and using the fact that $\mathbf{H}_i$ satisfies the Helmholtz equation written in Eq. (55).

The integration over the solid angle in Eq. (105) is done in a similar way as the integration in Eq. (94). The final result is

$$W_{ext} = -\frac{\pi|E_0|^2}{2\eta k^2}\sum_{l=1}^{\infty}\sum_{m=-1,+1}(2l+1)\mathrm{Re}\big\{ma_E(l,m)+a_M(l,m)\big\}. \tag{109}$$

In obtaining Eq. (109), we have used the Wronskian in Eq. (A22). The Wronskian, together with the Re{} operator that appears in Eq. (103), remove the dependence of W_{ext} on r.

Dividing Eq. (109) by the intensity of the incident light yields the extinction cross section

$$C_{ext} = -\frac{\pi}{k^2}\sum_{l=1}^{\infty}\sum_{m=-1,+1}(2l+1)\mathrm{Re}\big\{ma_E(l,m)+a_M(l,m)\big\}. \tag{110}$$

Similarly, we can get the absorption cross section by dividing W_a by the intensity of the incident light. From Eq. (106) we see that the absorption cross section is

$$C_a = C_{ext} - C_s. \tag{111}$$

Similar expressions for C_s, C_a and C_{ext} can be found in Ref. [17] which, however, correspond to a spherical scatterer.

The absorption cross section can be interpreted as an effective area, from which the scatterer takes energy off from the incident electromagnetic wave and converts it into other forms of energy, such as heat. The extinction cross section, on the other hand, can be interpreted as the total area, that removes energy from the incident light mode. Extinction can also be seen as the loss of energy due to the interference between the incident and the scattered light [20].

Equations (99), (110) and (111) enable us to use the multipole coefficients for calculating the interaction cross sections of individual scatterers. By studying these cross sections we obtain an additional insight into the way a certain structure interacts with light. When dealing with systems of several scatterers, this insight can help us to learn which effects are due to scattering by a single structure, and which due to an electromagnetic coupling between the structures.

If the scatterer has mirror symmetries, certain restrictions can be found on the values that the multipole coefficients can have. We consider a scatterer with a mirror symmetry with respect to both the $x = 0$ and the $y = 0$ plane. An x-polarized plane wave, described by Eq. (107), is incident on the scatterer. The scatterer can, for example, be a sphere, a cylinder illuminated from the top, or a cube with the facets parallel to the x-, y- and z-axes. If in addition, the scatterer is symmetric to a rotation by $\pi/2$ radians around the z-axis, the scattering is independent of the polarization of the incident plane wave. Obtaining this polarization independence is one of the main motivations for studying symmetric scatterers.

For a scatterer having the mirror symmetries mentioned above and interacting with an x-polarized plane wave, the scattered electric field must everywhere in the $x = 0$ plane be directed in the $\hat{\mathbf{x}}$ direction. Likewise, the scattered magnetic field must be directed in the $\hat{\mathbf{y}}$ direction everywhere in the $y = 0$ plane. In spherical

coordinates, these requirements imply that

$$\hat{\mathbf{r}} \cdot \mathbf{E}_s(r, \theta, \phi = \frac{\pi}{2}) = 0, \tag{112}$$

$$\hat{\theta} \cdot \mathbf{E}_s(r, \theta, \phi = \frac{\pi}{2}) = 0, \tag{113}$$

$$\hat{\mathbf{r}} \cdot \mathbf{H}_s(r, \theta, \phi = 0) = 0, \tag{114}$$

$$\hat{\theta} \cdot \mathbf{H}_s(r, \theta, \phi = 0) = 0. \tag{115}$$

As a consequence of the general properties of the associated Legendre polynomials P_l^m [17], the functions $O_{lm}P_l^m$, $O_{lm}\tau_{lm}$ and $O_{lm}\pi_{lm}$ in the multipole expansion in Eqs. (71)-(76) have the following symmetries in the azimuthal order m:

$$O_{l,-m}P_l^{-m}(\cos\theta) = (-1)^m O_{lm}P_l^m(\cos\theta), \tag{116}$$

$$O_{l,-m}\tau_{l,-m}(\theta) = (-1)^m O_{lm}\tau_{lm}(\theta), \tag{117}$$

$$O_{l,-m}\pi_{l,-m}(\theta) = (-1)^{m+1} O_{lm}\pi_{lm}(\theta). \tag{118}$$

Inserting Eqs. (117)-(118) into Eq. (113) yields

$$a_E(l, 0) = 0, \tag{119}$$

$$a_E(l, m) + a_E(l, -m) = 0, \tag{120}$$

$$a_M(l, m) - a_M(l, -m) = 0, \tag{121}$$

for $m > 0$. Likewise, inserting Eqs. (117)-(118) into Eq. (115) yields

$$a_M(l, 0) = 0, \tag{122}$$

$$a_E(l, m) + (-1)^{m+1} a_E(l, -m) = 0, \tag{123}$$

$$a_M(l, m) + (-1)^m a_M(l, -m) = 0. \tag{124}$$

Together Eqs. (119)-(124) state that, for the scatterer and the plane wave considered, the electric multipole coefficients satisfy the equation

$$a_E(l, -m) = -a_E(l, m), \tag{125}$$

for odd m and $a_E(l, m) = 0$ for even m. For the magnetic multipole coefficients we have

$$a_M(l, -m) = a_M(l, m), \tag{126}$$

for odd m and $a_M(l, m) = 0$ for even m. At the end of Sec. 3.2, the requirements in Eqs. (125) and (126) are related to the specific types of electric currents that can be excited in the symmetric scatterer.

3.2 Mapping between the multipole expansion and electric current excitations in meta-atoms

In Sec. 2.1, we described materials by treating each molecule as a point particle with electric and magnetic multipole moments. This enabled us to write a macroscopic electromagnetic theory, in which the average multipole moment densities act as electromagnetic field sources. We apply the same method for describing metamaterials and, likewise, treat each meta-atom as a point particle with electric and magnetic multipole moments. In this subsection we analyze the relation between the terms in our multipole expansion and the radiation generated by certain localized distributions of electric current. Furthermore, we rigorously map the electric dipole, electric quadrupole and magnetic dipole terms in the multipole expansion to point multipoles of electric current in the Cartesian coordinate system.

Often one distinguishes between the electric and magnetic multipoles. Electric multipoles, when used as field sources in electrostatics [17], are spatially fixed charge distributions. Magnetic multipoles, when used as field sources in magnetostatics [17], can be represented by electric current loops. In electrodynamics, both oscillating electric and magnetic multipoles can be seen as the sources of electromagnetic radiation. Alternatively, one can consider oscillating electric currents as the only source of radiation. It is useful to obtain an intuitive picture about the distributions of light-induced electric currents in meta-atoms, and therefore, we consider point elements of electric current as the only source of the radiation.

We first consider a current element of length L that carries a time-harmonic electric current with a complex amplitude $\mathbf{I}$. The element is positioned at the origin of the coordinate system in a homogeneous and isotropic dielectric with $\mu_r = 1$. The oscillating current emits radiation of a wavelength λ into the dielectric. We assume that $L << \lambda$. This allows us to treat the current element as a point element. For this point current element we write the complex amplitude of the current density as

$$\mathbf{J}_1(\mathbf{r}) = \mathbf{I}L\delta(\mathbf{r}). \tag{127}$$

Next, we consider two point current elements, in which the currents oscillate in opposite directions. One of the elements, with a current $+\mathbf{I}$, is displaced from the origin in the $\hat{\mathbf{x}}$ direction by a distance $s/2$. The other element, with a current $-\mathbf{I}$, is displaced in the opposite direction by the same distance, $s/2$. Using Eq. (127), we obtain the complex amplitude of the current density that describes these two current elements as

$$\mathbf{J}_2(\mathbf{r}) = -\mathbf{I}L\Big(\delta\big(x+\frac{s}{2}\big) - \delta\big(x-\frac{s}{2}\big)\Big)\delta(y)\delta(z). \tag{128}$$

If $s << \lambda$, we can treat this collection of two currents as a second-order point element. Considering s to be infinitesimally small in Eq. (128), but such that the product $\mathbf{I}Ls$ stays finite, and using the definition of the derivative, we obtain

$$\mathbf{J}_2(\mathbf{r}) = \varsigma(\hat{\mathbf{x}})\mathbf{J}_1(\mathbf{r}), \tag{129}$$

where the operator ς is defined as

$$\varsigma(\hat{\mathbf{u}}) = -s\frac{d}{du}. \tag{130}$$

Similar displacements can be done in the $\hat{\mathbf{y}}$ and $\hat{\mathbf{z}}$ directions, by applying the operators $\varsigma(\hat{\mathbf{y}})$ and $\varsigma(\hat{\mathbf{z}})$, respectively.

Even higher orders of the point current elements can be obtained by sequentially applying the operator in Eq. (130) to the current density of a lower-order point current element [19]. In Eq. (130), $\hat{\mathbf{u}}$ can be chosen as $\hat{\mathbf{x}}$, $\hat{\mathbf{y}}$, $\hat{\mathbf{z}}$ or any linear combination of them. The effect of the operator on a point current element can be seen as follows. The operator makes a copy of the point current element. The copy has a complex amplitude that is out of phase by π radians with respect to the original element. The original element is displaced, in the $\hat{\mathbf{u}}$ direction, by a distance of $s/2$. The copy is displaced in the $-\hat{\mathbf{u}}$ direction by the same distance, $s/2$. Finally, s is considered to be infinitesimally small.

The electric dipole moment of a continuous charge distribution is (compare to Eq. (6))

$$\mathbf{p} = \int \rho(\mathbf{r})\mathbf{r}d^3r. \tag{131}$$

Using the continuity equation (Eq. (22)) and partial integration, Eq. (131) can be written as

$$\mathbf{p} = \frac{i}{\omega}\int \mathbf{J}(\mathbf{r})d^3r. \tag{132}$$

The current element described by Eq. (127) can then be written as

$$\mathbf{J}_1(\mathbf{r}) = -i\omega\mathbf{p}\delta(\mathbf{r}). \tag{133}$$

The electric quadrupole moment of a continuous charge distribution is

$$\overleftrightarrow{\mathbf{q}} = \frac{1}{2}\int \rho(\mathbf{r})\mathbf{r}\mathbf{r}d^3r. \tag{134}$$

Using the continuity equation and partial integration yields

$$\overleftrightarrow{\mathbf{q}} = \frac{i}{2\omega}\int \Big(\mathbf{J}(\mathbf{r})\mathbf{r} + \mathbf{r}\mathbf{J}(\mathbf{r})\Big)d^3r. \tag{135}$$

The current configuration in Eq. (129) corresponds to an electric quadrupole moment. Choosing $\mathbf{I} = \hat{\mathbf{y}}I$ in Eq. (129) yields the same $\overleftrightarrow{\mathbf{q}} = (\hat{\mathbf{x}}\hat{\mathbf{y}} + \hat{\mathbf{y}}\hat{\mathbf{x}})iILs/(2\omega)$ as choosing $\mathbf{I} = \hat{\mathbf{x}}I$ and changing the operator to $\varsigma(\hat{\mathbf{y}})$. This is a consequence of $\overleftrightarrow{\mathbf{q}}$ being a symmetric dyadic. However, the fields generated by these current configurations are different. This difference can be examined after introducing the magnetic dipole moment

$$\mathbf{m} = \frac{1}{2}\int \mathbf{r}\times\mathbf{J}d^3r. \tag{136}$$

Then, the current configuration with $\mathbf{I} = \hat{\mathbf{y}}I$ has $\mathbf{m} = \hat{\mathbf{z}}ILs/2$, while the other one has $\mathbf{m} = -\hat{\mathbf{z}}ILs/2$. Using Eqs. (135) and (136), we can write Eq. (129) for any

choice of $\mathbf{I}$ and $\varsigma(\hat{\mathbf{u}})$ in the form

$$\mathbf{J}_2(\mathbf{r}) = i\omega \overleftrightarrow{\mathbf{q}} \cdot \nabla\delta(\mathbf{r}) - \mathbf{m} \times \nabla\delta(\mathbf{r}). \tag{137}$$

We see that the magnetic dipole moment and the electric quadrupole moment are current excitations of the same order.

When defining the electric multipoles from the charge distribution, one is forced to introduce magnetic multipoles in order to uniquely describe the radiation. Next, we define a new set of electric multipoles directly from the current density distribution. This set of multipoles is complete, and no additional magnetic multipoles are needed. Note that the multipole moment tensors obtained in this way are in general not symmetric. We define the current quadrupole moment as

$$\overleftrightarrow{\mathsf{Q}} = \frac{i}{\omega} \int \mathbf{J}(\mathbf{r}) \mathbf{r} d^3 r. \tag{138}$$

This $\overleftrightarrow{\mathsf{Q}}$ should not be confused with the macroscopic quadrupole moment density $\overleftrightarrow{\mathbf{Q}}$ in Sec. 2. We can now use Eq. (138) to write Eq. (129) for any choice of $\mathbf{I}$ and $\varsigma(\hat{\mathbf{u}})$ as

$$\mathbf{J}_2(\mathbf{r}) = i\omega \Big(\overleftrightarrow{\mathsf{Q}} \cdot \nabla \Big) \delta(\mathbf{r}). \tag{139}$$

Here, each element Q_{vu} of the current quadrupole dyadic describes a point current element constructed from a current element in the $\hat{\mathbf{v}}$ direction operated on by the operator $\varsigma(\hat{\mathbf{u}})$ in Eq. (130). Electric quadrupoles and magnetic dipoles can be decomposed into current quadrupoles. An example of such a decomposition is depicted in Fig. 1.

Higher order current multipoles are obtained by using the operator in Eq. (130). Because this operator commutes with itself, it only matters how many times it is used, e.g., with $\hat{\mathbf{u}} = \hat{\mathbf{x}}$. We define the current multipole moment of order l to be

$$\overleftrightarrow{\mathbf{M}}^{(l)} = \frac{i}{(l-1)!\omega} \int \mathbf{J}(\mathbf{r}) \mathbf{r}^{l-1} d^3 r, \tag{140}$$

where $\overleftrightarrow{\mathbf{M}}^{(l)}$ is a tensor of rank l. For the orders $l = 1, 2, ...$, the multipole is a dipole ($\overleftrightarrow{\mathbf{M}}^{(1)} = \mathbf{p}$), a quadrupole ($\overleftrightarrow{\mathbf{M}}^{(2)} = \overleftrightarrow{\mathsf{Q}}$), and so on. For $l > 2$, several elements of $\overleftrightarrow{\mathbf{M}}^{(l)}$ are equal. For example, the octopole moments are such that $M^{(3)}_{xyz} = M^{(3)}_{xzy}$.

The elements of $\overleftrightarrow{\mathbf{M}}^{(l)}$ can be mapped onto the coefficients $a_E(l,m)$ and $a_M(l,m)$ in our multipole expansion given in Eqs. (63) and (64). This implies mapping the multipole expansion of the current density in Cartesian coordinates onto the multipole expansion of electromagnetic fields in spherical coordinates. We start by making use of a circular coordinate system (w, w^*, z) (see A.4), where $w = (x + iy)/\sqrt{2}$ and w^* being its complex conjugate. The unit vectors in this system are $(\hat{\mathbf{w}}, \hat{\mathbf{w}}^*, \hat{\mathbf{z}})$, where $\hat{\mathbf{w}} = (\hat{\mathbf{x}} - i\hat{\mathbf{y}})/\sqrt{2}$ and $\hat{\mathbf{w}}^*$ being its complex conjugate. Because the transformation is linear, the operator ς in Eq. (130) still commutes with itself.

The elements of the current multipole tensors in the introduced circular coordinate system can be related to the elements in the Cartesian coordinate system by

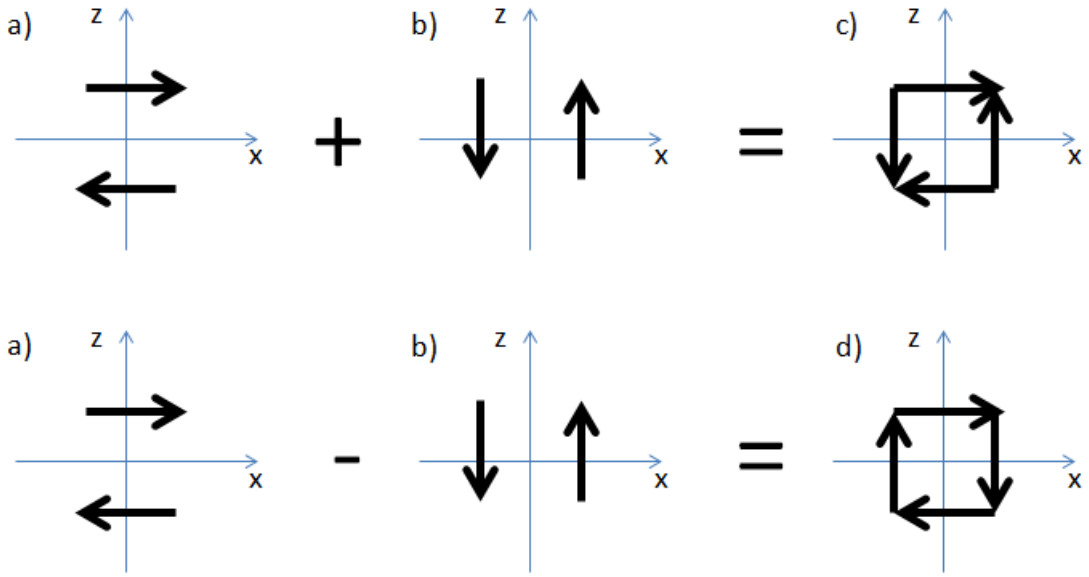

Figure 1: Decomposition of an electric quadrupole and magnetic dipole into current quadrupoles. Each bold arrow represents a time-harmonic electric current of complex amplitude I flowing through a wire of length L. The separation between the parallel wires is s. The moments are: a) $\overleftrightarrow{\mathsf{Q}} = \hat{\mathbf{x}}\hat{\mathbf{z}}iILs/\omega$, b) $\overleftrightarrow{\mathsf{Q}} = \hat{\mathbf{z}}\hat{\mathbf{x}}iILs/\omega$, c) $\overleftrightarrow{\mathbf{q}} = (\hat{\mathbf{x}}\hat{\mathbf{z}} + \hat{\mathbf{z}}\hat{\mathbf{x}})iILs/\omega$ and $\mathbf{m} = 0$, d) $\overleftrightarrow{\mathbf{q}} = 0$ and $\mathbf{m} = \hat{\mathbf{y}}ILs$.

using vector projections. In complex coordinates, the projection of a tensor $\overleftrightarrow{\mathbf{a}}$ onto the unit vector $\hat{\mathbf{w}}$ is $\overleftrightarrow{\mathbf{a}} \cdot \hat{\mathbf{w}}^*$. For current dipoles and quadrupoles the relations are

$$p_w = \frac{1}{\sqrt{2}}\big(p_x + ip_y\big), \tag{141}$$

$$\mathsf{Q}_{zw} = \frac{1}{\sqrt{2}}\big(\mathsf{Q}_{zx} + i\mathsf{Q}_{zy}\big), \tag{142}$$

$$\mathsf{Q}_{wz} = \frac{1}{\sqrt{2}}\big(\mathsf{Q}_{xz} + i\mathsf{Q}_{yz}\big), \tag{143}$$

$$\mathsf{Q}_{ww} = \frac{1}{2}\big(\mathsf{Q}_{xx} - \mathsf{Q}_{yy} + i\big(\mathsf{Q}_{xy} + \mathsf{Q}_{yx}\big)\big), \tag{144}$$

$$\mathsf{Q}_{ww^*} = \frac{1}{2}\big(\mathsf{Q}_{xx} + \mathsf{Q}_{yy} - i\big(\mathsf{Q}_{xy} - \mathsf{Q}_{yx}\big)\big). \tag{145}$$

The remaining elements of these moments are obtained from Eqs. (141)-(145) by replacing w's with w^*'s, w^*'s with w's and all explicitly written i's with $-i$'s.

The multipole expansion of the current density in circular coordinates, obtained by repeatedly applying the operator ς to (133), can be written as

$$\begin{aligned}\mathbf{J}(\mathbf{r}) =& i\omega \sum_{l=1}^{\infty} \sum_{\hat{\mathbf{v}}=\{\hat{\mathbf{w}},\hat{\mathbf{w}}^*,\hat{\mathbf{z}}\}} \sum_{a=0}^{l-1} \sum_{b=0}^{l-a-1} M(l,\hat{\mathbf{v}},a,b)\hat{\mathbf{v}} \\ & \frac{(-1)^l(l-1)!}{a!b!(l-(a+b+1))!} \frac{d^a}{dw^a} \frac{d^b}{dw^{*b}} \frac{d^{l-(a+b+1)}}{dz^{l-(a+b+1)}} \delta(\mathbf{r}),\end{aligned} \tag{146}$$

where $M(l,\hat{\mathbf{v}},a,b)$ are the elements of $\overleftrightarrow{\mathbf{M}}^{(l)}$ describing a multipole obtained by applying the operator $\varsigma(\hat{\mathbf{u}})$ to a $\hat{\mathbf{v}}$-oriented current element a times with $\hat{\mathbf{u}}=\hat{\mathbf{w}}$, b times with $\hat{\mathbf{u}}=\hat{\mathbf{w}}^*$ and $l-(a+b+1)$ times with $\hat{\mathbf{u}}=\hat{\mathbf{z}}$. The coefficients in Eq. (146) are chosen such that the elements of the multipole tensors are consistent with Eq. (140).

To solve for the electromagnetic fields radiated by the current density distribution in Eq. (146), we define the vector potential $\mathbf{A}$ through

$$\mathbf{H}(\mathbf{r})=\frac{1}{\mu_0}\nabla\times\mathbf{A}(\mathbf{r}). \tag{147}$$

In the Lorenz gauge, $\mathbf{A}$ satisfies the wave equation [17]

$$\big(\nabla^2+k^2\big)\mathbf{A}(\mathbf{r})=-\mu_0\mathbf{J}(\mathbf{r}). \tag{148}$$

For the electric current element in Eq. (133), the solution for the wave equation is [17]

$$\mathbf{A}_1(\mathbf{r})=\frac{1}{\omega}\frac{k^3\mathbf{p}}{4\pi\epsilon}h_0^{(1)}(kr), \tag{149}$$

where $\epsilon=\epsilon_0\epsilon_r$ is the electric permittivity of the surrounding isotropic and homogeneous dielectric.

The multipole expansion of the vector potential is obtained by applying the operator ς to Eq. (148) with $\mathbf{J}=\mathbf{J}_1$ and $\mathbf{A}=\mathbf{A}_1$, until $\mathbf{J}$ becomes that in Eq. (146). Since the spatial differential operators in both Cartesian and circular coordinates commute with ∇^2, we obtain the multipole expansion for $\mathbf{A}$ from the left hand side of Eq. (148) as

$$\begin{aligned}\mathbf{A}(\mathbf{r})=&\frac{1}{\omega}\frac{k^3}{4\pi\epsilon}\sum_{l=1}^{\infty}\sum_{\hat{\mathbf{v}}=\{\hat{\mathbf{w}},\hat{\mathbf{w}}^*,\hat{\mathbf{z}}\}}\sum_{a=0}^{l-1}\sum_{b=0}^{l-a-1}M(l,\hat{\mathbf{v}},a,b)\hat{\mathbf{v}}\\&\frac{(-1)^{l-1}(l-1)!}{a!b!(l-(a+b+1))!}\frac{d^a}{dw^a}\frac{d^b}{dw^{*b}}\frac{d^{l-(a+b+1)}}{dz^{l-(a+b+1)}}h_0^{(1)}(kr).\end{aligned} \tag{150}$$

The magnetic field corresponding to Eq. (150) is given by Eq. (147). Outside the source, we use Eqs. (43) and (148) to obtain the electric field

$$\mathbf{E}(\mathbf{r})=i\omega\Big(\mathbf{A}(\mathbf{r})+\frac{1}{k^2}\nabla\big(\nabla\cdot\mathbf{A}(\mathbf{r})\big)\Big). \tag{151}$$

In the following calculations in this subsection, the equations in A.3 and A.4 are used frequently. The various derivatives of the Hankel function in Eq. (150) complicate the calculation of $\mathbf{E}$ and $\mathbf{H}$. For our meta-atoms it is enough to consider the current dipoles ($l=1$) and current quadrupoles ($l=2$). Neglecting the $l>2$ terms enables us to write Eq. (150) as

$$\begin{aligned}\mathbf{A}(\mathbf{r})=&\frac{1}{\omega}\frac{1}{4\pi\epsilon}\sum_{l=1}^{2}\sum_{\hat{\mathbf{v}}=\{\hat{\mathbf{w}},\hat{\mathbf{w}}^*,\hat{\mathbf{z}}\}}\sum_{a=0}^{l-1}\sum_{b=0}^{l-a-1}M(l,\hat{\mathbf{v}},a,b)\hat{\mathbf{v}}k^{l+2}\\&e^{i(b-a)\phi}\Big(\frac{\sin\theta}{\sqrt{2}}\Big)^{a+b}\big(\cos\theta\big)^{l-(a+b+1)}h_{l-1}^{(1)}(kr).\end{aligned} \tag{152}$$

Next, we insert Eq. (152) into Eq. (151) to obtain the electric field. The radial part of the obtained electric field can be expressed in the form

$$E_r(\mathbf{r}) = \frac{i}{4\pi\epsilon}\sum_{l=1}^{2}\sum_{\hat{\mathbf{v}}=\{\hat{\mathbf{w}},\hat{\mathbf{w}}^*,\hat{\mathbf{z}}\}}\sum_{a=0}^{l-1}\sum_{b=0}^{l-a-1} M(l,\hat{\mathbf{v}},a,b)k^{l+2}e^{i(b-a)\phi}\Big(\frac{\sin\theta}{\sqrt{2}}\Big)^{a+b}\big(\cos\theta\big)^{l-(a+b+1)}$$
$$\Big(\hat{\mathbf{v}}\cdot\hat{\mathbf{w}}^*\frac{e^{-i\phi}}{\sqrt{2}}\big((l+1)\sin\theta-\frac{2b}{\sin\theta}\big)+\hat{\mathbf{v}}\cdot\hat{\mathbf{w}}\frac{e^{i\phi}}{\sqrt{2}}\big((l+1)\sin\theta-\frac{2a}{\sin\theta}\big)$$
$$+\hat{\mathbf{v}}\cdot\hat{\mathbf{z}}\big((l+1)\cos\theta-\frac{l-(a+b+1)}{\cos\theta}\big)\Big)\frac{h_l^{(1)}(kr)}{kr}. \tag{153}$$

When evaluating the terms of this equation one can use $\hat{\mathbf{w}}\cdot\hat{\mathbf{w}}^*=1$ and $\hat{\mathbf{w}}\cdot\hat{\mathbf{w}}=0$. From Eq. (153) it is seen that certain quadrupoles, such as $M(2,\hat{\mathbf{w}},0,0)=\mathsf{Q}_{wz}$ and $M(2,\hat{\mathbf{z}},1,0)=\mathsf{Q}_{zw}$, produce the same radial electric field.

The radial part of the magnetic field is obtained by inserting Eq. (152) into Eq. (147). For the current quadrupoles ($l=2$), we obtain

$$H_r(\mathbf{r}) = \frac{i}{4\pi\epsilon\eta}\sum_{\hat{\mathbf{v}}=\{\hat{\mathbf{w}},\hat{\mathbf{w}}^*,\hat{\mathbf{z}}\}}\sum_{a=0}^{1}\sum_{b=0}^{1-a} M(2,\hat{\mathbf{v}},a,b)k^{4}e^{i(b-a)\phi}\Big(\frac{\sin\theta}{\sqrt{2}}\Big)^{a+b}\big(\cos\theta\big)^{-a-b}$$
$$\Big(\hat{\mathbf{v}}\cdot\hat{\mathbf{w}}^*\frac{e^{-i\phi}}{\sqrt{2}}\big((1-a+b)\sin\theta-\frac{2b}{\sin\theta}\big)+\hat{\mathbf{v}}\cdot\hat{\mathbf{w}}\frac{e^{i\phi}}{\sqrt{2}}\big(-(1+a-b)\sin\theta+\frac{2a}{\sin\theta}\big)$$
$$+\hat{\mathbf{v}}\cdot\hat{\mathbf{z}}(b-a)\cos\theta\Big)\frac{h_1^{(1)}(kr)}{kr}. \tag{154}$$

For the current dipoles ($l=1$), we have $H_r=0$. This is a direct consequence of the fact that the oscillating electric current element is indistinguishable from an oscillating electric point dipole. Electric multipoles, by definition, do not produce any radial magnetic field. Higher order current multipoles, such as current quadrupoles, are superpositions of oscillating electric and magnetic multipoles and can therefore have a radial magnetic field.

The multipole coefficients $a_E(l,m)$ are obtained by inserting the radial field in Eq. (153) into Eq. (79). For each choice of l, $\hat{\mathbf{v}}$, a and b the angular dependence of E_r can be written as a spherical harmonic. Using the orthogonality in Eq. (66), we obtain

$$a_E(1,m) = \frac{-ik^3}{6\pi\epsilon E_0}\sqrt{2}\big(\delta_{m,0}p_z+\delta_{m,-1}p_w-\delta_{m,1}p_{w^*}\big), \tag{155}$$

$$a_E(2,m) = \frac{-k^4}{20\pi\epsilon E_0}\Big(\sqrt{\frac{2}{3}}\delta_{m,0}\big(2\mathsf{Q}_{zz}-\mathsf{Q}_{ww^*}-\mathsf{Q}_{w^*w}\big)+\sqrt{2}\delta_{m,-1}\big(\mathsf{Q}_{wz}+\mathsf{Q}_{zw}\big)$$
$$-\sqrt{2}\delta_{m,1}\big(\mathsf{Q}_{w^*z}+\mathsf{Q}_{zw^*}\big)+2\delta_{m,-2}\mathsf{Q}_{ww}+2\delta_{m,2}\mathsf{Q}_{w^*w^*}\Big). \tag{156}$$

Similarly, $a_M(l,m)$ are obtained by inserting the radial field in Eq. (154) into

Eq. (80). We obtain

$$a_M(1,m) = \frac{k^4}{12\pi\epsilon E_0}\sqrt{2}\Big(\delta_{m,0}\big(\mathsf{Q}_{w^*w}-\mathsf{Q}_{ww^*}\big)+\delta_{m,-1}\big(\mathsf{Q}_{wz}-\mathsf{Q}_{zw}\big)+\delta_{m,1}\big(\mathsf{Q}_{w^*z}-\mathsf{Q}_{zw^*}\big)\Big). \tag{157}$$

In Eqs. (155), (156) and (157) we present the current moments of the lowest-order multipole expansion coefficients expressed in circular coordinates. The current moments can be mapped to Cartesian coordinates by using Eqs. (141)-(145). Doing this, we obtain

$$a_E(1,m) = \frac{-ik^3}{6\pi\epsilon E_0}\big(\sqrt{2}\delta_{m,0}p_z + \delta_{m,-1}(p_x+ip_y) - \delta_{m,1}(p_x-ip_y)\big), \tag{158}$$

$$\begin{aligned} a_E(2,m) = \frac{-k^4}{20\pi\epsilon E_0}\Big(&\sqrt{\frac{2}{3}}\delta_{m,0}\big(2\mathsf{Q}_{zz}-\mathsf{Q}_{xx}-\mathsf{Q}_{yy}\big)\\ &+\delta_{m,-1}\big(\mathsf{Q}_{xz}+\mathsf{Q}_{zx}+i(\mathsf{Q}_{yz}+\mathsf{Q}_{zy})\big)\\ &-\delta_{m,1}\big(\mathsf{Q}_{xz}+\mathsf{Q}_{zx}-i(\mathsf{Q}_{yz}+\mathsf{Q}_{zy})\big)\\ &+\delta_{m,-2}\big(\mathsf{Q}_{xx}-\mathsf{Q}_{yy}+i(\mathsf{Q}_{xy}+\mathsf{Q}_{yx})\big)\\ &+\delta_{m,2}\big(\mathsf{Q}_{xx}-\mathsf{Q}_{yy}-i(\mathsf{Q}_{xy}+\mathsf{Q}_{yx})\big)\Big), \end{aligned} \tag{159}$$

$$\begin{aligned} a_M(1,m) = \frac{k^4}{12\pi\epsilon E_0}\Big(&i\sqrt{2}\delta_{m,0}\big(\mathsf{Q}_{xy}-\mathsf{Q}_{yx}\big)+\delta_{m,-1}\big(\mathsf{Q}_{xz}-\mathsf{Q}_{zx}\\ &+i(\mathsf{Q}_{yz}-\mathsf{Q}_{zy})\big)+\delta_{m,1}\big(\mathsf{Q}_{xz}-\mathsf{Q}_{zx}-i(\mathsf{Q}_{yz}-\mathsf{Q}_{zy})\big)\Big). \end{aligned} \tag{160}$$

Equations (158)-(160) establish relations between the Cartesian current moments and the multipole coefficients. It can be seen that only 8 quadrupole coefficients (5 electric quadrupoles and 3 magnetic dipoles) are used in the multipole expansion, whereas there are 9 elements in the Cartesian quadrupole dyadic. This is because the spherically symmetric excitation with $\mathsf{Q}_{xx} = \mathsf{Q}_{yy} = \mathsf{Q}_{zz}$ does not generate any electromagnetic field. This can be verified by using Eqs. (151) and (152). Thus, the 9th quadrupole equation is

$$\mathsf{Q}_{xx} + \mathsf{Q}_{yy} + \mathsf{Q}_{zz} = 0. \tag{161}$$

In Sec. 4, we study scatterers that exhibit mirror symmetries with respect to both the $x = 0$ and $y = 0$ plane. Previously, we have determined the multipole coefficients $a_E(l,m)$ and $a_M(l,m)$ which are non-zero for such scatterers. We can therefore insert the obtained Eqs. (125) and (126) into Eqs. (158)-(160) to find the types of current dipoles and quadrupoles that can be excited in such a scatterer. Using also Eq. (161), one can see that most of the current moments are equal to zero, and only the moments p_x, Q_{xz} and Q_{zx} can be excited. In the following, we study the possibility to efficiently excite the quadrupoles Q_{xz} and Q_{zx} in a symmetric meta-atom.

3.3 Quasistatic dipole-dipole model

Electromagnetic excitations in small scatterers of simple geometry, such as spheres or discs, are mostly of an electric dipole character. Therefore, in order to excite a current quadrupole, one should use either a particle with a more complicated geometry or a pair of simple, e.g., spherical, particles. We call such pairs of particles metadimers, if their sizes are much smaller than the radiation wavelength. If opposite currents are excited in the two scatterers of such a metadimer, we obtain a current quadrupole. In the following, we consider a metadimer where the axis joining the two scatterers, the dimer axis, is chosen to be the z-axis. If the metadimer is symmetric with respect to a rotation by $\pi/2$ around the dimer axis, the optical power scattered by the dimer is independent of the polarization of the incident light that propagates along this axis. It is therefore enough to consider, for example, an incident x-polarized plane wave that can excite the current quadrupole moment Q_{xz}. A metadimer is depicted in Fig. 2.

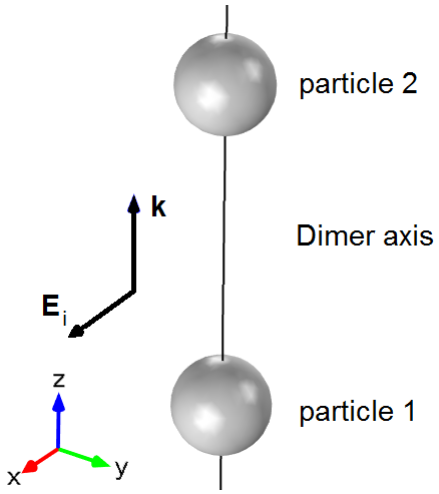

Figure 2: Illustration of a metadimer. The incident electric field $\mathbf{E}_i$ can excite the current quadrupole moment Q_{xz}.

Let us first develop a simple quasistatic dipole-dipole model to describe the excitation of the Q_{xz} moment in a metadimer. Since the metadimer is much smaller in size than the wavelength, the electric field of the incident plane wave can be considered as a field with a constant phase across the metadimer volume. The individual scatterers are assumed to have simple geometries and, therefore, we can assume that an x-polarized electric field, $\hat{\mathbf{x}}E_j$, only excites a dipole moment

$$\mathbf{p}_j = \hat{\mathbf{x}}\alpha_j E_j, \tag{162}$$

in each of the scatterers, $j = 1, 2$. In Eq. (162), α_j is a complex-valued electric dipole polarizability of the scatterer j. If $\mathbf{p}_1 = -\mathbf{p}_2$, the currents in the two scatterers oscillate in opposite directions resulting in a Q_{xz} quadrupole excitation in the metadimer. Then, the total dipole moment is $\mathbf{p} = \mathbf{p}_1 + \mathbf{p}_2 = 0$.

In the quasistatic dipole-dipole model, we approximate each scatterer in the metadimer by a point dipole on the z-axis, which also interacts with the field scattered by the other scatterer. The first point dipole ($j = 1$) is assumed to be located at $z = 0$, whereas the second one ($j = 2$) is at $z = d$. Using Eqs. (149) and (151) for an x-oriented dipole yields the scattered field of the first dipole evaluated at the second dipole as

$$\mathbf{E}_{1s}(r = d, \theta = 0) = \frac{ik^3\mathbf{p}_1}{4\pi\epsilon}\big(h_0^{(1)}(kd) - \frac{h_1^{(1)}(kd)}{kd}\big). \tag{163}$$

Since $kd << \pi$, the exponential functions in the spherical Hankel functions are $e^{ikd} \approx 1$. Furthermore, after writing the explicit forms of h_l in Eq. (163), the term on the order of $(kd)^{-3}$ dominates over the $(kd)^{-2}$ and $(kd)^{-1}$ terms. In the quasistatic limit, Eq. (163) becomes

$$\mathbf{E}_{1s}(r = d, \theta = 0) = -\frac{\mathbf{p}_1}{4\pi\epsilon d^3}, \tag{164}$$

which indicates that the near-field of dipole 1 at the position of dipole 2 is opposite to $\mathbf{p}_1$. Due to symmetry, the near-field of dipole 2 at the position of dipole 1 is

$$\mathbf{E}_{2s}(r = 0) = -\frac{\mathbf{p}_2}{4\pi\epsilon d^3}. \tag{165}$$

The electric field of the incident plane wave is $\mathbf{E}_i = E_0\hat{\mathbf{x}}$ at the metadimer. Thus, the total electric fields at dipoles 1 and 2 are $\mathbf{E}_1 = \mathbf{E}_i + \mathbf{E}_{2s}(r = 0)$ and $\mathbf{E}_2 = \mathbf{E}_i + \mathbf{E}_{1s}(r = d, \theta = 0)$, respectively. Insertion of Eqs. (164) and (165) into Eq. (162) yields two coupled equations

$$p_1 = \alpha_1\big(E_0 - Cp_2\big), \tag{166}$$

$$p_2 = \alpha_2\big(E_0 - Cp_1\big), \tag{167}$$

where the factor $C = 1/(4\pi\epsilon d^3)$ is a positive constant. The solution for p_1 is

$$p_1 = \tilde{\alpha}_1 E_0, \tag{168}$$

where the effective polarizability of dipole 1 is

$$\tilde{\alpha}_1 = \frac{1 - C\alpha_2}{1 - C^2\alpha_1\alpha_2}\alpha_1. \tag{169}$$

The corresponding equations for p_2 are obtained by interchanging the indices 1 and 2. From Eq. (169) we see that the near-field interaction between the dipoles modifies their effective polarizabilites (with respect to the incident wave).

Using Eqs. (110) and (158), we obtain the extinction cross section of a single x-polarized dipole as

$$C_{ext} = \frac{k}{\epsilon}\mathrm{Im}\Big\{\frac{p_x}{E_0}\Big\}, \tag{170}$$

which states that the imaginary part of the electric dipole polarizability describes the extinction. In Eq. (12.50) of Ref. [26], the quantity C_{ext} is called the absorption cross section. This is because Ref. [26] neglects the radiation reaction. Equation (170) is consistent with Ref. [27]. Using Eqs. (99) and (158) yields the scattering cross

section of the x-polarized dipole as

$$C_s = \frac{k^4}{6\pi\epsilon^2}\frac{|p_x|^2}{|E_0|^2}, \tag{171}$$

which states that the absolute value of the electric dipole polarizability describes the scattering. Equation (171) is consistent with Eq. (12.49) in Ref. [26]. Since the scattering does not generate energy, all cross sections C_s, C_a and C_{ext} are positive. Equations (162) and (170) then state that α_1 and α_2 must be complex numbers with positive imaginary parts. Therefore, without the near-field interaction, the two dipoles can never be exactly out of phase and $p_1 \neq -p_2$. However, the near-field interaction enables the fact that at least one of the dipoles can have an effective polarizability $\tilde{\alpha}_j$ with a negative imaginary part, as long as the metadimer as a whole has $C_a \geq 0$.

Requiring $p_1 = -p_2$ yields

$$\frac{1}{\alpha_1} + \frac{1}{\alpha_2} = 2C, \tag{172}$$

which can never be completely satisfied in the quasistatic dipole-dipole model, as C is real in this model and both α_1 and α_2 have positive imaginary parts. Furthermore, Eqs. (111), (170) and (171) imply that, for a single dipole, C_a is proportional to $\mathrm{Im}\{\alpha_j\} - k^3|\alpha_j|^2/(6\pi\epsilon)$. Since $C_a \geq 0$, it follows that a large $|\alpha_j|^2$ requires a large $\mathrm{Im}\{\alpha_j\}$. This result, together with Eq. (172), shows that for efficient scatterers, such as resonant metallic particles, the metadimer necessarily has a non-zero dipolar response. For less efficient scatterers, such as glass particles, α_1 and α_2 have negligible imaginary parts. However, we also found out that for such particles the real part of α is small and positive, which leads to a very large required C in Eq. (172). A large C, in turn, requires a very small separation d between the particles. This contradicts the assumption that the scatterers can be seen as point dipoles, as then the near-field of one particle varies throughout the volume of the other particle.

We notice that the assumptions of the quasistatic dipole-dipole model do not allow obtaining a pure quadrupole excitation in a metadimer. Therefore, we seek for a dimer structure where the separation d is so small that the dipole-dipole model is no longer valid. We can still use the quasistatic model to assess the values of α_1, α_2 and d which yield a close match to Eq. (172). The solutions of Eq. (172) for α_1 and the corresponding dipole moment p_1 are

$$\alpha_1 = \frac{1}{2C - \frac{1}{\alpha_2}}, \tag{173}$$

$$p_1 = \frac{\alpha_1}{1 - C\alpha_1}E_0. \tag{174}$$

Similar solutions can be written for the second scatterer by interchanging the indices 1 and 2 in Eqs. (173) and (174). If we are interested in a considerable quadrupole excitation, then in addition to the condition $p_1 \approx -p_2$, we require $|p_1|$ to be as large as possible. To maximize the modulus of p_1 in Eq. (174), we choose $\mathrm{Re}\{\alpha_1\}$ to be close to C^{-1}. To obtain $p_1 \approx -p_2$, we choose $\mathrm{Re}\{\alpha_1\}$ slightly below C^{-1} and $\mathrm{Re}\{\alpha_2\}$ slightly above C^{-1}, such that Eq. (173) is satisfied. However, if the products

$\mathrm{Re}\{\alpha_j\}C$ are too close to unity, the positive imaginary parts of α_j dominate in the denominator of Eq. (174), which makes both $\tilde{\alpha}_1 = p_1/E_0$ and $\tilde{\alpha}_2 = p_2/E_0$ have essentially equal phases.

Using Eqs. (158) and (162), one can see that the condition $\mathrm{Re}\{\alpha_1\} = C^{-1}$ implies that the multipole coefficient $a_E(1,1)$ satisfies the equation

$$\mathrm{Im}\{a_E(1,1)\} = \frac{2}{3}(kd)^3. \tag{175}$$

If we know the multipole coefficients describing the scattering by a single scatterer, then Eq. (175) can be used to estimate the required interparticle distance in a metadimer. Furthermore, one scatterer should be tuned to have $\mathrm{Im}\{a_E(1,1)\}$ slightly smaller than the one used in Eq. (175), while the second scatterer should have the value of $\mathrm{Im}\{a_E(1,1)\}$ slightly larger.

3.4 Displaced electric dipoles

The quasistatic dipole-dipole model shows that in a metadimer there can be excited nearly oppositely oscillating electric currents. What is left to show, is that these opposite currents indeed radiate as a Q_{xz} current quadrupole, resulting in non-zero multipole coefficients $a_E(2,\pm1)$ and $a_M(1,\pm1)$. We define the origin of the coordinate system to be between the two x-oriented dipoles, such that dipole 1 is at $z = -d/2$ and dipole 2 at $z = d/2$ on the z-axis. We then calculate the coefficients of the multipole expansion given in Eqs. (63) and (64).

The electric field produced by a single electric dipole ($\mathbf{p} = p\hat{\mathbf{x}}$) that is located at the coordinate system origin, is obtained by using Eqs. (63) and (158) to be

$$\mathbf{E}(r,\theta,\phi) = -\frac{ik^3}{2\sqrt{6\pi}\epsilon} p\big(\mathbf{N}_{11}(\mathbf{r}) - \mathbf{N}_{1,-1}(\mathbf{r})\big), \tag{176}$$

where the second solenoidal spherical vector wave function is

$$\mathbf{N}_{lm}(\mathbf{r}) = \frac{-i\sqrt{l(l+1)}}{k}\nabla \times \big(h_l^{(1)}(kr)\mathbf{X}_{lm}(\theta,\phi)\big). \tag{177}$$

If the dipole is displaced to $z = \mp d/2$, the electric field can be written in the same form as in Eq. (176), but with $\mathbf{N}_{lm}(\mathbf{r})$ being replaced with a translated $\mathbf{N}_{lm}(\mathbf{r}\pm\hat{\mathbf{z}}d/2)$. The multipole expansion for the displaced dipole can be obtained by expanding $\mathbf{N}_{lm}(\mathbf{r} \pm \hat{\mathbf{z}}d/2)$ as

$$\mathbf{N}_{lm}(\mathbf{r} \pm \hat{\mathbf{z}}\frac{d}{2}) = \sum_{n=1}^{\infty}\sum_{p=-n}^{n}\Big(B^{\pm}_{l,m,n,p}\mathbf{M}_{np}(\mathbf{r}) + A^{\pm}_{l,m,n,p}\mathbf{N}_{np}(\mathbf{r})\Big), \tag{178}$$

where the first solenoidal spherical vector wave function is

$$\mathbf{M}_{lm}(\mathbf{r}) = -i\sqrt{l(l+1)}h_l^{(1)}(kr)\mathbf{X}_{lm}(\theta,\phi). \tag{179}$$

The means to calculate the expansion coefficients $A^{\pm}_{l,m,n,p}$ and $B^{\pm}_{l,m,n,p}$ in Eq. (178) are presented in Ref. [28]. Using Eqs. (176) and (178), the electric field due to both

dipole 1 (displaced by $-d/2$) and dipole 2 (displaced by $+d/2$) is

$$\mathbf{E}(\mathbf{r}) = -\frac{ik^3}{2\sqrt{6\pi\epsilon}}\sum_{l=1}^{\infty}\sum_{m=-l}^{l}\Big(\big(p_1(B^+_{1,1,l,m} - B^+_{1,-1,l,m}) + p_2(B^-_{1,1,l,m} - B^-_{1,-1,l,m})\big)\mathbf{M}_{lm}(\mathbf{r}) + \big(p_1(A^+_{1,1,l,m} - A^+_{1,-1,l,m}) + p_2(A^-_{1,1,l,m} - A^-_{1,-1,l,m})\big)\mathbf{N}_{lm}(\mathbf{r})\Big), \tag{180}$$

where p_j is the dipole moment of dipole j. Equation (180) is the multipole expansion describing the radiation of an idealized metadimer. Comparing this expansion with the expansion in Eq. (63), we obtain the multipole coefficients

$$a_E(l,m) = \frac{\sqrt{l(l+1)}k^3}{i^{l+2}2\sqrt{6(2l+1)}\pi\epsilon E_0}\big(p_1(A^+_{1,1,l,m} - A^+_{1,-1,l,m}) + p_2(A^-_{1,1,l,m} - A^-_{1,-1,l,m})\big), \tag{181}$$

$$a_M(l,m) = \frac{\sqrt{l(l+1)}k^3}{i^{l+2}2\sqrt{6(2l+1)}\pi\epsilon E_0}\big(p_1(B^+_{1,1,l,m} - B^+_{1,-1,l,m}) + p_2(B^-_{1,1,l,m} - B^-_{1,-1,l,m})\big). \tag{182}$$

Then we use Eqs. (46), (74) and (75) in Ref. [28] to calculate these coefficients. Equation (67) in Ref. [28] gives the same coefficients A. However, in Ref. [28], Eq. (68) yields incorrect real-valued coefficients B, while Eq. (75) yields correct imaginary-valued B. After a rather lengthy calculation, including the use of Eq. (A15), we obtain

$$A^+_{1,1,l,1} = (-1)^l\sqrt{\frac{3}{2l(l+1)(2l+1)}}\big(lj_{l+1}(k\frac{d}{2}) - (l+1)j_{l-1}(k\frac{d}{2})\big), \tag{183}$$

$$A^-_{1,1,l,1} = (-1)^{l+1}A^+_{1,1,l,1}, \tag{184}$$

$$A^\pm_{1,-1,l,-1} = A^\pm_{1,1,l,1}, \tag{185}$$

$$B^+_{1,1,l,1} = i(-1)^{l+1}\sqrt{\frac{3(2l+1)}{2l(l+1)}}j_l(k\frac{d}{2}), \tag{186}$$

$$B^-_{1,1,l,1} = (-1)^l B^+_{1,1,l,1}, \tag{187}$$

$$B^\pm_{1,-1,l,-1} = -B^\pm_{1,1,l,1}. \tag{188}$$

All other coefficients are equal to zero. Thus, displacement of a dipole from the origin generates radiation of higher-order moments, but it preserves the orders of m. The displacement can not, for example, yield a non-zero $a_E(1,0)$ that would correspond to a z-oriented dipole.

We assume that the metadimer is much smaller than the radiation wavelength. Since now $kd << \pi$, we can expand the spherical Bessel functions in the small argument limit. We neglect terms of higher order than $(kd)^1$. In this limit, the lowest-order spherical Bessel functions are $j_0(kd/2) = 1$ and $j_1(kd/2) = kd/6$, while all higher-order ones are equal to zero [17]. Inserting Eqs. (183)-(188) into Eqs. (181)

and (182), we obtain

$$a_E(1,m) = \frac{ik^3}{6\pi\epsilon E_0}(p_1+p_2)(\delta_{m,1}-\delta_{m,-1}), \tag{189}$$

$$a_E(2,m) = \frac{k^4 d}{40\pi\epsilon E_0}(p_2-p_1)(\delta_{m,1}-\delta_{m,-1}), \tag{190}$$

$$a_M(1,m) = \frac{k^4 d}{24\pi\epsilon E_0}(p_2-p_1)(\delta_{m,1}+\delta_{m,-1}), \tag{191}$$

with all the other coefficients being equal to zero.

Finally, we insert Eqs. (189)-(191) into Eqs. (158)-(160) and solve for the current moments. The only non-zero current moments are

$$p_x = p_1 + p_2, \tag{192}$$

$$\mathsf{Q}_{xz} = \frac{(p_2-p_1)d}{2}. \tag{193}$$

The result in Eqs. (192) and (193) proves that the radiation of two electric dipoles, oscillating out of phase and displaced from the origin in opposite directions, is of a quadrupole character. To obtain the criterion for the quadrupole scattering to dominate over the dipole scattering, we insert Eqs. (189)-(191) into Eq. (99). The scattered energy in the Q_{xz} mode dominates over that of the p_x mode when

$$|p_1+p_2| < \frac{kd}{\sqrt{10}}|p_2-p_1|. \tag{194}$$

Equation (194) indicates that for small metadimers, $kd << \pi$, the phase difference between p_1 and p_2 should be close to π in order to obtain a dominant quadrupole scattering. Since we consider metadimers made of noble metals, which at optical frequencies exhibit large temporal dispersion, we expect a dominant quadrupole scattering to be possible only in some specific spectral range, in which $\mathrm{Re}\{p_1\} \approx -\mathrm{Re}\{p_2\}$ and $\mathrm{Im}\{p_1\} \approx -\mathrm{Im}\{p_2\}$.

4 Numerical calculations

In this section, we present numerical studies of visible light scattering by meta-atoms. The electromagnetic excitations in the meta-atoms are analyzed by using the multipole expansion described in sections 2 and 3. We start this section by considering a single disc-shaped particle made of silver. Then, searching for significant higher order excitations, we combine two of such discs to form a metadimer. Finally, we consider one- and two-dimensional arrays of metadimers to assess the possibility of creating a quadrupole metamaterial.

The calculations have been performed with the help of a computer software COMSOL Multiphysics, version 4.2.1.166, which makes use of the finite element method to solve the Maxwell equations. The calculated values of the electric field were further processed with a MATLAB software, version R2011a.

4.1 Silver disc

We begin by studying light scattering by a single disc made of silver. The disc has a cylindrical geometry, in which the height is smaller than the diameter. Such structures can be fabricated by using simple planar fabrication methods, such as optical interference lithography [29, 30] and hole-mask colloidal lithography [31]. Also, for plane wave illumination along the disc axis, the scattering does not depend on the polarization of the incident light. Thus, metal nanodiscs are promising elements for realizing polarization independent metamaterials and devices. In order to have a scenario that can be realized in practice, the considered discs are embedded in a dielectric medium.

The coordinate system is chosen such, that the disc has its symmetry axis oriented along the z-axis and the origin is located at the center of the disc. We choose the surrounding dielectric to have a relative electric permittivity $\epsilon_{r,d} = 2.25$, which is that of ordinary glass. The disc is illuminated by a linearly x-polarized plane wave that is propagating in the $\hat{\mathbf{z}}$ direction. Thus, $\mathbf{E}_i$ in Eq. (91) is given by Eq. (107), where $k = 2\pi\sqrt{\epsilon_{r,d}}/\lambda_0$ and $\lambda_0 = 2\pi c/\omega$ is the wavelength in vacuum. At visible frequencies, the permittivity of silver depends strongly on λ_0. For the relative electric permittivity of silver, we use the values obtained in Ref. [32].

By subtracting the incident field $\mathbf{E}_i$ from the total field in Eq. (91), we obtain the scattered field $\mathbf{E}_s$. The scattered field is expanded with the multipole expansion in Eq. (63). We numerically evaluate the expansion coefficients $a_E(l,m)$ and $a_M(l,m)$, using two alternative methods, one based on Eqs. (78) and (79) and the other on Eqs. (89) and (90). For consistency, we require that both methods yield the same results. The source current in Eqs. (89) and (90) is obtained by inserting the total field, $\mathbf{E}_i + \mathbf{E}_s$, into Eq. (93). Equations (99), (110) and (111) are used to calculate the interaction cross sections.

If the disc is to be used as a constituent of a homogeneous metamaterial, it is required that the disc size is much smaller than the wavelength of light. We consider visible light, with a vacuum wavelength being larger than 400 nm. The homogeneity condition $kD << \pi$ for a linear dimension D implies that $D <<$

130 nm. We consider discs with a diameter ranging between 30 and 40 nm and thus, a metamaterial consisting of these discs can only conditionally be considered as homogeneous. On the other hand, if the disc is parallel to the light wavefront, then the disc thickness, h, should satisfy the condition $kh << \pi$. The thickness of each disc is chosen to be 10 nm.

The scattering cross sections of silver discs, with a radius ranging between 15 and 20 nm, are depicted in Fig. 3. For each disc, a localized surface plasmon resonance occurs at a certain wavelength, which leads to enhanced scattering. This resonance red-shifts with increasing disc radius. The absorption cross sections of the discs are depicted in Fig. 4. The surface plasmon resonance also leads to enhanced absorption. By comparing Fig. 3 and Fig. 4, we see that the scattering cross section scales with the radius more rapidly than the absorption cross section. As a consequence, for very small particles, absorption dominates scattering. A dominating absorption causes a dominating imaginary part of the electric dipole polarizability (see Sec. 3.3), which can prevent us from exciting a dominating current quadrupole in a paired-disc metadimer.

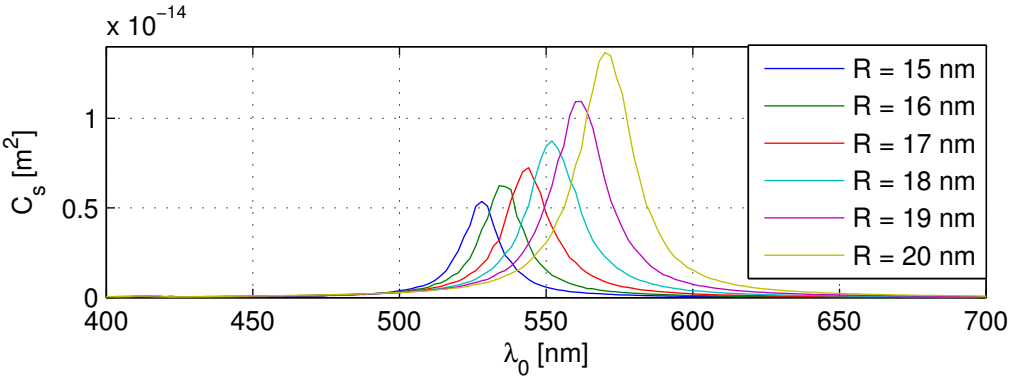

Figure 3: Spectra of the scattering cross sections of individual silver discs. The discs are 10 nm thick, have a radius R and are embedded in glass.

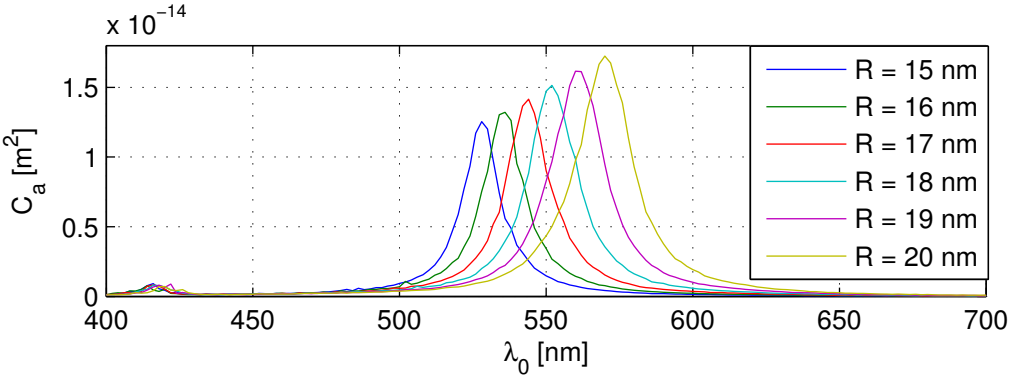

Figure 4: Spectra of the absorption cross sections of individual silver discs. The discs are 10 nm thick, have a radius R and are embedded in glass.

We have found that the only non-zero multipole coefficients obtained for a single disc are the $a_E(1,1) = -a_E(1,-1)$ coefficients. Thus, the scattering is completely explained by an x-oriented electric dipole excitation, p_x. This is a consequence of the small size and the rotational symmetry of the discs (see the discussion at the end of Sec. 3.2).

Our target is to combine two discs into a metadimer, which could possess a Q_{xz} excitation. The electric dipole moment p_x is obtained from $a_E(1,1)$ by using Eq. (158). For the discs with radii of 15 and 20 nm, the dipole moments normalized to the amplitude of the incident electric field, p_x/E_0, are depicted in Fig. 5. We notice that increasing the disc radius from 15 to 20 nm results in a red-shift of the spectral response and increase of the dipole moment. We have found that, for small changes of the disc radius, the $a_E(1,1)$ coefficient scales linearly with the radius. Then, as follows from Eq. (99), the scattering cross section, plotted in Fig. 3, has a quadratic dependence on the disc radius.

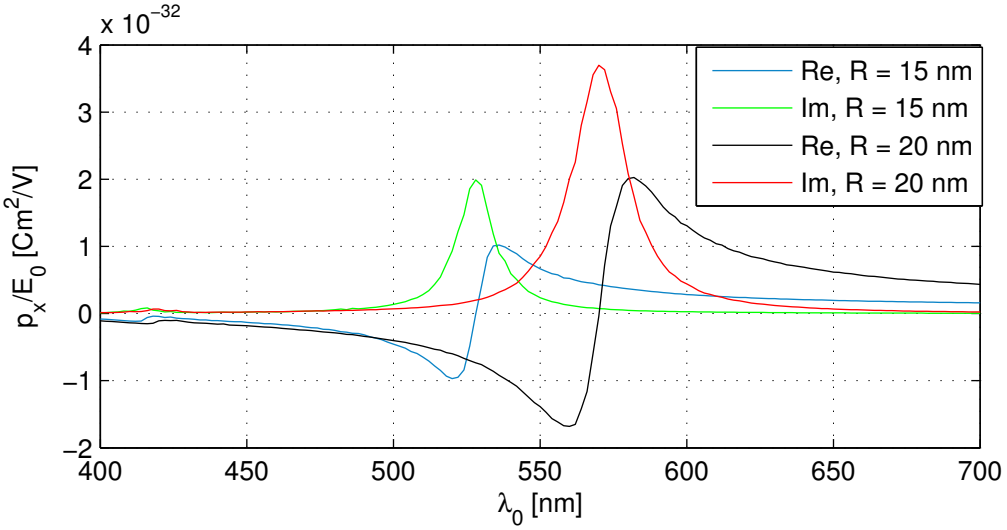

Figure 5: Spectra of the x-components of the excited dipole moments in silver discs, normalized to the incident electric field amplitude. The discs are 10 nm thick, have a radius R and are embedded in glass. The real and imaginary parts are plotted separately.

Within the quasistatic dipole-dipole model, the quantities in Fig. 5 are the real and imaginary parts of the electric dipole polarizability. In Sec. 3.3, we concluded that, in order to obtain a dominant Q_{xz} scattering, the polarizability of each scatterer should be essentially real and positive. This indicates that, using these discs, a dominant Q_{xz} scattering can be obtained at wavelengths around 600 nm. At 600 nm wavelength, the disc with a radius of 15 nm has $\mathrm{Im}\{a_E(1,1)\} = 0.03$, and the disc with a radius of 20 nm has $\mathrm{Im}\{a_E(1,1)\} = 0.13$. Using Eq. (175) we obtain the point-dipole separation distances $d = 23$ nm and $d = 37$ nm for the discs with a radius of 15 nm and 20 nm, respectively. These distances are positive and much smaller than the wavelength of light, which indicates that a metadimer with dominant Q_{xz} scattering is possible.

4.2 The disc metadimer

Two silver discs, with their axes coinciding with the z-axis, are positioned to have a small gap between them. The structure as a whole is much smaller than the wavelength of light, and as such, the disc pair can be seen as a metadimer. This metadimer is depicted in Fig. 6. We consider the same plane wave illumination as for the discs in the previous subsection. The multipole expansion of the scattered light is performed with respect to the coordinate system origin, which is chosen to lie on the z-axis at the center of the gap between the discs. Because of the chosen illumination direction (from above), we call the discs in the $z < 0$ and $z > 0$ half-space as the upper and lower disc, respectively.

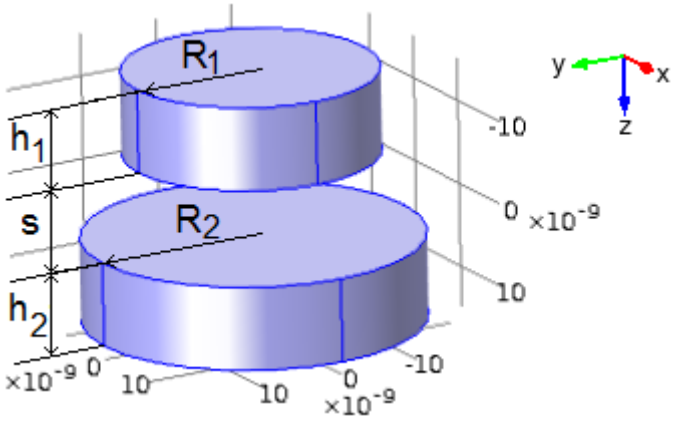

Figure 6: Illustration of a disc metadimer. In this example, the dimensions are $(R_1,h_1,R_2,h_2,s) = (15,10,20,10,10)$ in nm.

We choose the upper disc to have a radius R_1 of 15 nm and a thickness h_1 of 10 nm. In order to obtain opposite currents in the discs, it is important to have the two discs different in size. Therefore, the lower disc is chosen to have a radius R_2 of 20 nm, but the same thickness $h_2 = h_1$. We consider that the discs have a surface-to-surface separation s of 30 nm. Thus, the dimensions of the dimer in nanometers are $(R_1,h_1,R_2,h_2,s) = (15,10,20,10,30)$. Because of the dimer's size and geometry, all moments of higher order than the electric quadrupole and the magnetic dipole moments are negligible. This is confirmed by our numerical calculations.

Due to symmetry, we only have to consider the coefficients $a_E(1,1) = -a_E(1,-1)$, $a_M(1,1) = a_M(1,-1)$ and $a_E(2,1) = -a_E(2,-1)$. Based on Eq. (99), we can then define the scattering cross sections per excitation mode in the metadimer as

$$C_s^e = \frac{6\pi}{k^2}|a_E(1,1)|^2, \tag{195}$$

$$C_s^m = \frac{6\pi}{k^2}|a_M(1,1)|^2, \tag{196}$$

$$C_s^q = \frac{10\pi}{k^2}|a_E(2,1)|^2. \tag{197}$$

The modal cross sections C_s^e, C_s^m and C_s^q describe how much electromagnetic energy is scattered due to the electric dipole, magnetic dipole and electric quadrupole mode.

If C_s^m or C_s^q is greater than C_s^e, the current excitation resembles that of an ideal current quadrupole. In these cases we say that we have dominant Q-scattering.

The modal cross sections of the considered metadimer are depicted in Fig. 7. At a vacuum wavelength of 546 nm, the electric dipole moment is suppressed and the scattering is dominated by the electric quadrupole and the magnetic dipole. The lower plot in Fig. 7 shows that the energy scattered by the electric dipole mode is one order of magnitude lower than the energy scattered by the electric quadrupole and magnetic dipole modes. For this metadimer, the magnetic dipole scattering cross section is larger than the electric quadrupole one by a factor of approximately 1.7. This factor can be understood by resorting to Eqs. (99), (159) and (160) with the current quadrupole $\overleftrightarrow{\mathsf{Q}} = \mathsf{Q}_{xz}\hat{\mathbf{x}}\hat{\mathbf{z}}$. One then obtains a factor of 5/3, and any deviation from this factor is explained by the presence of a Q_{zx} moment. We conclude that, around the vacuum wavelength of 546 nm, the metadimer shows a dominant Q-scattering.

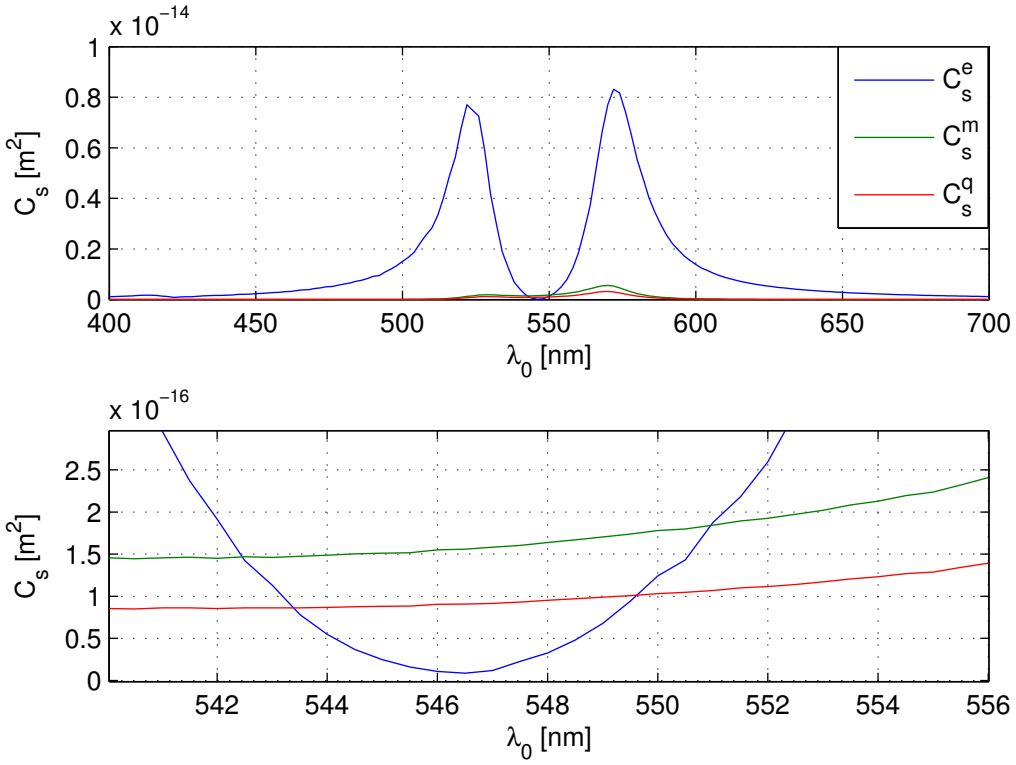

Figure 7: Spectra of the modal scattering cross sections of a silver metadimer. The metadimer is embedded in glass and has the dimensions (R_1,h_1,R_2,h_2,s) = (15,10,20,10,30), in nm. Upper plot: the whole visible spectrum, plotted with a spectral resolution of 2 nm. Lower plot: enlarged view around 546 nm, plotted with a spectral resolution of 0.5 nm.

To obtain an intuitive picture about the electric current distribution in the metadimer, we calculate the multipole coefficients for the individual discs, while they are assembled as the metadimer. This is done by using the integrals of the

source current density in Eqs. (89) and (90). We position the coordinate system origin at the center of one of the discs and perform the integration in Eqs. (89) and (90) only over the volume holding that disc. We find that the individual discs behave as electric dipoles, with $a_E(1,1) = -a_E(1,-1)$ being the only non-zero coefficients. The magnitudes and phases of p_x/E_0 for the individual discs are depicted in Fig. 8.

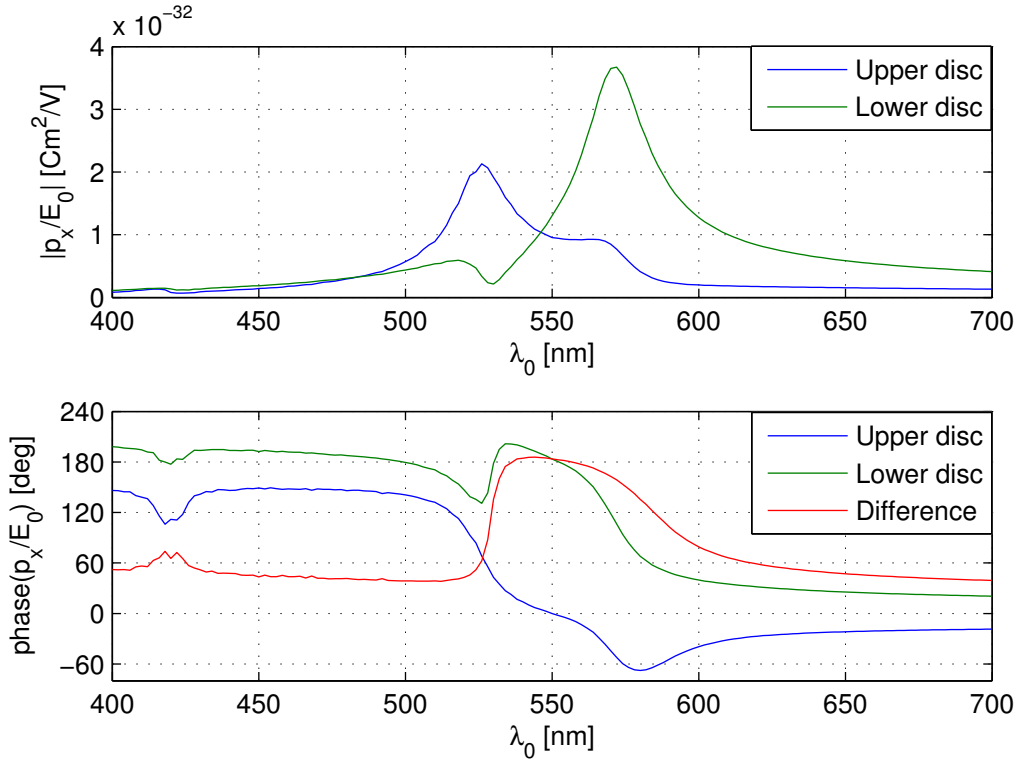

Figure 8: Spectra of the x-components of the excited dipole moments in the individual silver discs in the metadimer, normalized to the electric field amplitude of the incident light at the metadimer center. The metadimer is embedded in glass and has the dimensions (R_1,h_1,R_2,h_2,s) = (15,10,20,10,30), in nm. Upper plot: absolute value. Lower plot: phase in degrees.

The plots in Fig. 8 can be used to understand the properties of the electric currents in the individual discs. Note that the size of the metadimer is large enough to cause a propagation phase delay between the discs, which is visible in the lower plot in Fig. 8. This plot also shows that, for the longer wavelengths, the dipole moments in both discs are in phase with the incident field. Note the propagation phase delay mentioned above. The upper plot in Fig. 8 shows that there is an electric dipole resonance at a wavelength around 530 nm for the upper disc and around 575 nm for the lower disc. At shorter wavelengths, the discs' dipole moments are out of phase with the incident field. Thus, a spectral region exists between the resonances - at around 550 nm wavelength - where the dipole moments of the two discs are out of phase with each other. A dominant Q_{xz} scattering is obtained if, in addition, the two dipole moments have equal amplitudes. This can be seen from Eq. (194), where $kd/\sqrt{10} \approx 0.2$. From the upper plot in Fig. 8 we see that the

magnitudes of the dipole moments are equal at around a wavelength of 546 nm, which is in agreement with the plots in Fig. 7.

The wavelength of suppressed dipole scattering differs from that predicted in Sec. 3.3. By comparing Figs. 5 and 8, we see that, at a wavelength of 546 nm, the disc with a radius of 20 nm has an out-of-phase dipole moment (with respect to the incident field) even without the presence of the other disc. This contrasts with the quasistatic dipole-dipole model, which suggested that both particles in a metadimer should have positive polarizabilities in the absence of the other particle. We conclude that the quasistatic model yields inaccurate predictions due to the discs being too large compared to their separation distance to be treated as point dipoles.

We found out that reducing the separation between the two discs has the effect of red-shifting the wavelength of the dominant Q-scattering. Thus, the separation can be used as a parameter for tuning the Q-scattering wavelength. The modal scattering cross sections for a metadimer with a surface-to-surface separation of 10 nm are depicted in Fig. 9. For this separation, the dominant Q-scattering occurs at a wavelength of 594 nm.

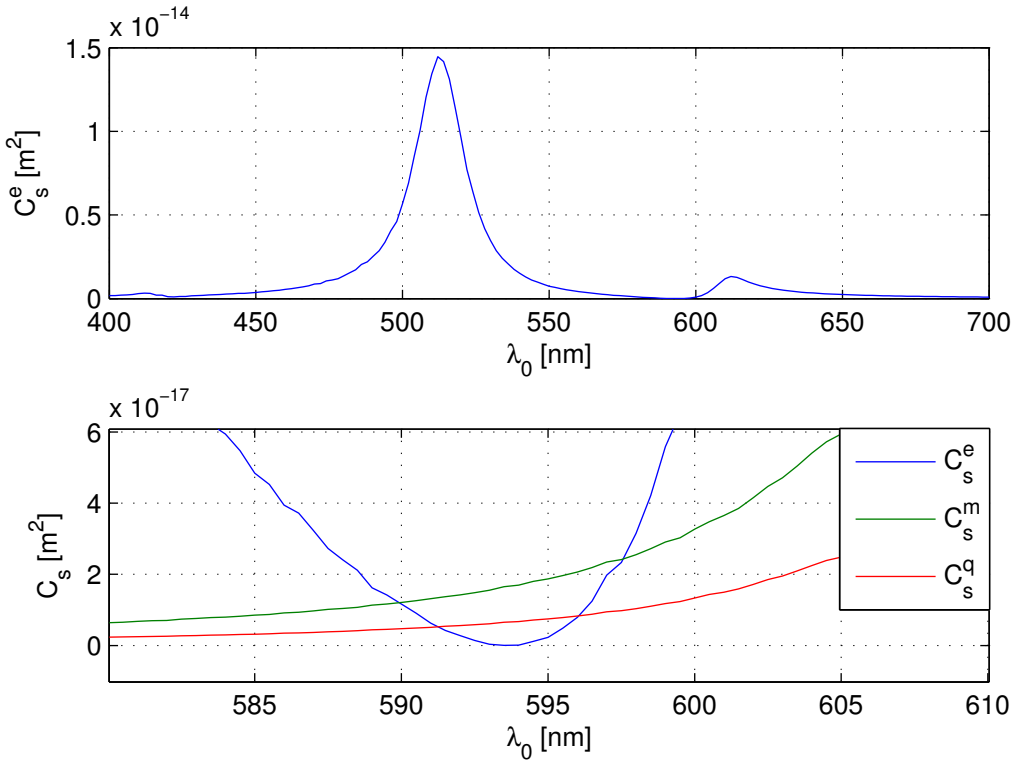

Figure 9: Spectra of the modal scattering cross sections of a silver metadimer. The metadimer is embedded in glass and has the dimensions $(R_1,h_1,R_2,h_2,s) = (15,10,20,10,10)$, in nm. Upper plot is for the electric dipole mode, plotted with a spectral resolution of 2 nm. Lower plot is for the three lowest-order modes around 594 nm, plotted with a spectral resolution of 0.5 nm.

The lower plot in Fig. 9 indicates that the Q-scattering is two orders of magnitude larger than the electric dipole scattering. However, we estimate that the inaccuracy in the numerically evaluated fields can be on the order of a few percentages, and therefore, we can only make a conclusion that C_s^m and C_s^q are at least one order of magnitude larger than C_s^e. We also note that C_s^m is larger than C_s^q by a factor in the range of 2.4-2.7. This means that we have a considerable contribution from the moment Q_{zx}. This is a consequence of the fact that the discs have a thickness comparable to the separation distance between the discs, which leads to a current distribution resembling more of a loop current than a Q_{xz} quadrupole, i.e., $|\mathsf{Q}_{xz} - \mathsf{Q}_{zx}| > |\mathsf{Q}_{xz} + \mathsf{Q}_{zx}|$. We can therefore say that the dimer is more magnetic than electric.

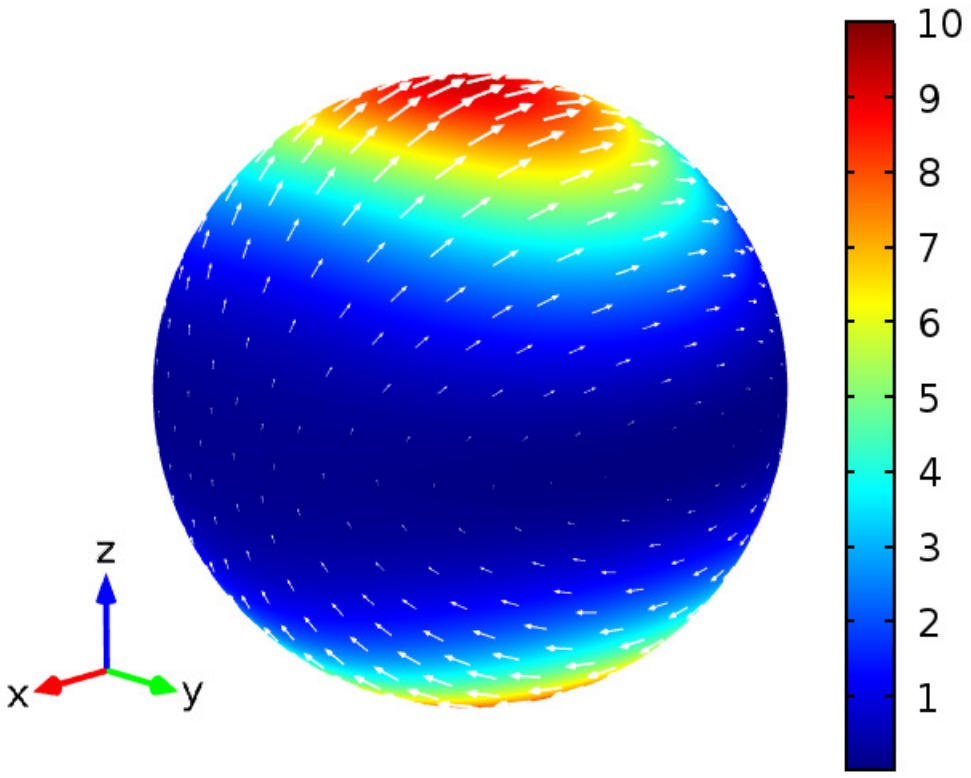

Figure 10: Far-field radiation pattern of a silver metadimer as plotted on a spherical surface. The metadimer is embedded in glass and has the dimensions (R_1,h_1,R_2,h_2,s) = (15,10,20,10,10), in nm. The illumination wavelength is $\lambda_0 = 593.5$ nm. Arrows: electric far-field vectors at $\omega t = \pi/2$. Colors: normalized far-field radiation energy. The incident field is x-polarized.

As the scattering is dominated by the electric quadrupole and magnetic dipole modes, it is expected that the far-field radiation pattern is different from that of an electric dipole mode. By using Eqs. (159) and (160), we find that the Q_{xz} mode has $a_E(2,1) = -a_E(2,-1) = 3a_M(1,1)/5 = 3a_M(1,-1)/5$. The complex amplitude of the electric far-field is found by inserting these coefficients into Eq. (63) and

neglecting the terms that decay faster than $1/r$ with increasing r. We obtain

$$\mathbf{E}_F^{\mathsf{Q}}(\mathbf{r}) = \frac{-ik^3 \mathsf{Q}_{xz}}{4\pi\epsilon} \frac{e^{ikr}}{r} \cos\theta \big(\hat{\theta}\cos\theta\cos\phi - \hat{\phi}\sin\phi\big). \tag{198}$$

Similarly, we can calculate the complex amplitude of the electric far-field of the p_x mode and obtain

$$\mathbf{E}_F^{p}(\mathbf{r}) = \frac{k^2 p_x}{4\pi\epsilon} \frac{e^{ikr}}{r} \big(\hat{\theta}\cos\theta\cos\phi - \hat{\phi}\sin\phi\big). \tag{199}$$

While the electric dipole radiates symmetrically around its axis, the current quadrupole radiates primarily in the $+\hat{\mathbf{z}}$ and $-\hat{\mathbf{z}}$ directions. Furthermore, the fields radiated in the $+\hat{\mathbf{z}}$ and $-\hat{\mathbf{z}}$ directions are out of phase with respect to each other. The far-field radiation pattern of a metadimer at the wavelength of dominant Q-scattering is depicted in Fig. 10. We notice that the electric far-field pattern deviates slightly from the pattern given by Eq. (198) due to the contribution from the Q_{zx} mode.

4.3 Particle arrays

We have found that a disc metadimer can provide dominant Q-scattering. In view of constructing quadrupole metamaterials, it is of interest to analyze the interaction of light with an array of such metadimers. If, in an array, the metadimers are positioned close to each other, they inevitably interact, which alters the electromagnetic excitations in each of them. In this subsection we consider infinite one- and two-dimensional arrays of metadimers.

We start by considering an infinitely long chain of identical silver disc metadimers. The metadimers are axis-aligned parallel to the z-axis and positioned side-by-side. The z-axis is directed such that the upper discs of the metadimers are located in the $z < 0$ half-space and the lower discs in the $z > 0$ half-space. We consider the same x-polarized plane wave illumination as in the previous subsection. If the chain is aligned along the $\hat{\mathbf{x}}$ direction the illumination is TM-polarized (transverse magnetic), since the incident plane wave has the *magnetic* field in the $\hat{\mathbf{y}}$ direction. Similarly, if the chain is aligned in the $\hat{\mathbf{y}}$ direction the illumination is TE-polarized (transverse electric). For an arbitrary orientation of the chain in the xy-plane, we can decompose the incident light into TE- and TM-polarized components. Because the chain is infinite, the metadimers are indistinguishable and the electric current density distributions must be identical in all of them.

We consider metadimers with the dimensions (R_1,h_1,R_2,h_2,s) = (15,10,20,10,10) in a chain of period P. The gap between neighboring upper discs is $P - 30$ nm and for the lower discs it is $P - 40$ nm. Because of the chain's symmetry, we can still use the modal cross sections of Eqs. (195)-(197). Now the electric field at a single metadimer is a superposition of the electric field of the original plane wave and the electric field of the light scattered by all other metadimers. Thus, the scattering cross section, as calculated using Eq. (99), loses its original meaning. We can, however, use Eqs. (195)-(197) as a measure of the relative strengths of the multipole excitations in the individual metadimers. The multipole coefficients have the same

meaning as previously: they describe the local distribution of the electric current in each metadimer.

The electric dipole scattering cross section for metadimers in a chain of period P, under TM-polarized illumination, are depicted in Fig. 11. In the limit of $P \to \infty$, the metadimers can be seen as independent scatterers, and therefore each of them has a spectrum depicted in the upper plot of Fig. 9. For these uncoupled metadimers the electric dipole scattering cross section has a peak value equal to 1.4×10^{-14} m^2 at a vacuum wavelength of 512 nm. From Fig. 11 we see that, at $P = 80$ nm (blue curve), the coupling between the metadimers red-shifts the electric dipole peak to 524 nm. The value at the peak is equal to 0.3×10^{-14} m^2, which is significantly smaller than the value for the uncoupled metadimers. Further reduction of the period increases the coupling between the neighboring metadimers, which, as depicted in Fig. 11, results in spectral red-shift and reduction of the peak of the electric dipole. Note, however, that the density of the metadimers increases, which partly compensates for the decrease of the overall response of the chain to the field.

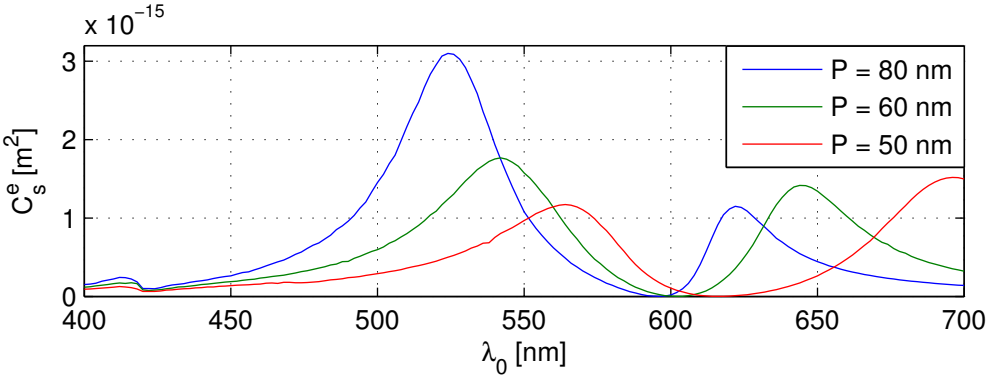

Figure 11: Spectra of the electric dipole scattering cross section of silver metadimers in an infinitely long chain of period P under TM-polarized illumination. The metadimers are embedded in glass and have the dimensions $(R_1,h_1,R_2,h_2,s) = (15,10,20,10,10)$, in nm.

From Fig. 11 we see that the electric dipole excitation is greatly suppressed at a wavelength of 596 nm for $P = 80$ nm, 602 nm for $P = 60$ nm, and 616 nm for $P = 50$ nm. Around these wavelengths, the metadimers exhibit dominant Q-scattering with similar spectra as in Fig. 9. For the three chosen values of P, the electric dipole scattering cross section C_s^e is, within the accuracy of the numerical solutions, one order of magnitude smaller than C_s^m and C_s^q. We conclude that the coupling under TM-polarized illumination does not disable the dominant Q$-$scattering. Instead, it red-shifts its spectral location.

Next, we consider the case of TE-polarization of the incident light. The electric dipole scattering cross section of metadimers in a chain of period P are depicted in Fig. 12. At a period of 80 nm, the electric dipole peak is at a vacuum wavelength of 502 nm. This peak is seen to be blue-shifted with respect to the uncoupled metadimer. The peak value, being equal to 0.8×10^{-14} m^2, is lower than for the uncoupled metadimers. Further reduction of the period, as depicted in Fig. 12,

results in further blue-shift and reduction of the electric dipole peak. Both the spectral shift and the peak-value reduction are smaller than for the case of TM-polarized illumination. Thus, the coupling of the metadimers under TM-polarized illumination has a more pronounced effect on the scattering than the coupling under TE-polarized illumination.

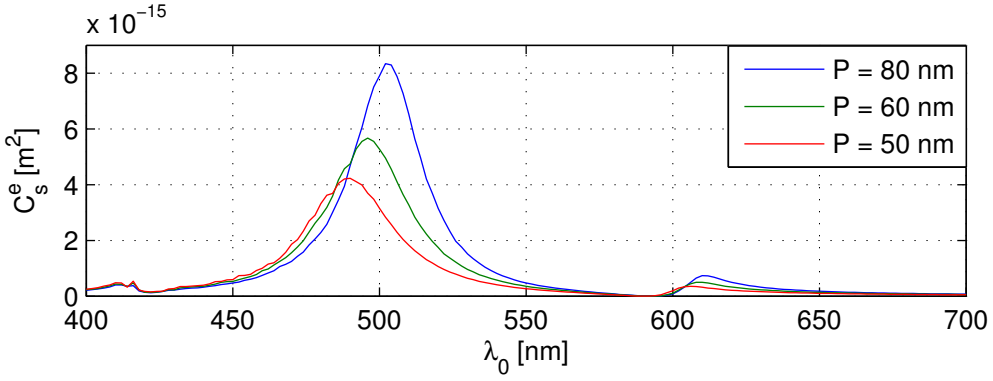

Figure 12: Spectra of the electric dipole scattering cross section of silver metadimers in an infinitely long chain of period P under TE-polarized illumination. The metadimers are embedded in glass and have the dimensions (R_1,h_1,R_2,h_2,s) = (15,10,20,10,10), in nm.

Also the spectral location of the electric dipole suppression exhibits a small blue-shift. From Fig. 12 we see that the electric dipole excitation is suppressed at the wavelength of 594 nm for $P = 80$ nm, 592 nm for $P = 60$ nm, and 590 nm for $P = 50$ nm. In the spectral region of the dipole suppression, the metadimers exhibit dominant Q-scattering. We again find that, similarly to the case of TM-polarized illumination, the cross section C_s^e is one order of magnitude smaller than the cross sections C_s^m and C_s^q. We therefore conclude that the coupling of the metadimers under TE-polarized illumination does not disable the dominant Q-scattering.

Finally, we consider scattering of light by a two-dimensional array of metadimers. The metadimers are axis-aligned along the z-axis and placed in a square lattice, such that the periodicity in the $\hat{\mathbf{x}}$ and $\hat{\mathbf{y}}$ directions have the same value P. The array is infinite, spanning the whole xy-plane. The illumination is the same as previously. In a two-dimensional array, each metadimer exhibits coupling not only in the directions perpendicular to $\mathbf{E}_i$ and $\mathbf{H}_i$ (TE and TM), but also in diagonal directions.

The electric dipole scattering cross section of metadimers in a square lattice of period P are depicted in Fig. 13. At $P = 80$ nm, the peak value of C_s^e is equal to 0.2×10^{-14} m^2. This low peak value is explained by the combined effect of coupling in both the TE and TM directions in the array. For the three periods of 80, 60 and 50 nm, the wavelengths at which the dipole suppression occurs closely match with those of the corresponding metadimer chains under TM-polarized illumination. We therefore conclude that it is primarily the coupling in the TM direction that red-shifts the location of the dipole suppression region.

The modal scattering cross sections for the square lattice with $P = 50$ nm, in the spectral region of the electric dipole suppression, are depicted in Fig. 14. We notice

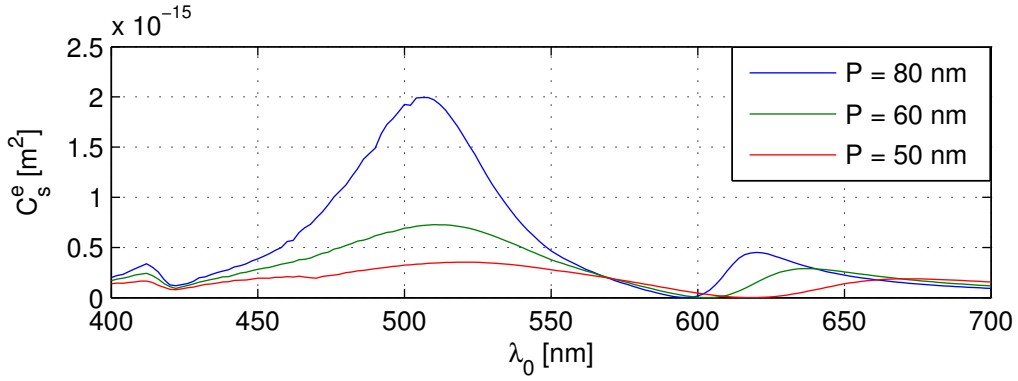

Figure 13: Spectra of the electric dipole scattering cross section of silver metadimers in a two-dimensional square lattice of period P. The metadimers are embedded in glass and have the dimensions (R_1,h_1,R_2,h_2,s) = (15,10,20,10,10), in nm.

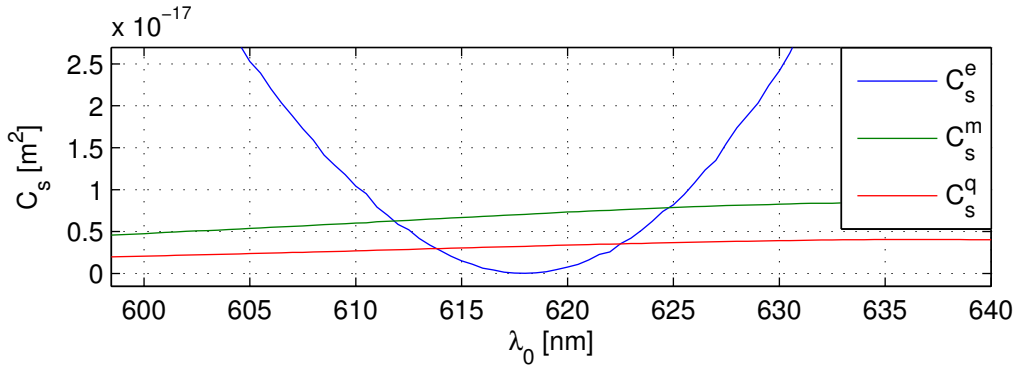

Figure 14: Spectra of the modal cross sections of a silver metadimer in a two-dimensional square lattice of period $P = 50$ nm. The metadimers are embedded in glass and have the dimensions (R_1,h_1,R_2,h_2,s) = (15,10,20,10,10), in nm. The plotted spectral resolution is 0.5 nm.

that in the spectral region around the wavelength of 618 nm, the cross section C_s^e is one order of magnitude smaller than C_s^m and C_s^q. The ratio between C_s^m and C_s^q is in the range of 2.1-2.3, which indicates that the contribution from the Q_{zx} excitation is still considerable, but smaller than for an uncoupled metadimer. We conclude that a dominant Q-scattering is obtainable also in two-dimensional arrays of metadimers. To our knowledge, dominant Q-scattering of visible light by such small structures as our metadimers has not been introduced previously in the literature.

Let us consider the wavelength of 618 nm, where the electric dipole excitation is minimized (see Fig. 14). The source current density, as calculated by Eq. (93), was found to lag/lead the incident field $\mathbf{E}_i$ by a phase of $\pi/2$ in the lower/upper disc. The source current density in one of the metadimers at $\omega t = \pi/2$ is shown by arrows in Fig. 15. The current excitation visually resembles that of the Q_{xz} mode. The slight curvature of the currents is interpreted as the contribution from the Q_{zx} mode. The net source current in the structure as a whole is equal to zero and

therefore no electric dipole moment is excited. In Fig. 15, we have also plotted the magnitude of the complex magnetic field normalized to that of the incident wave. We see that the magnetic field between the discs is localized and enhanced. This magnetic near-field is created by the opposite currents and lags the incident field in phase by $\pi/2$. Enhanced magnetic near-fields have been found previously in paired discs that, however, were much larger in size than our metadimers [33].

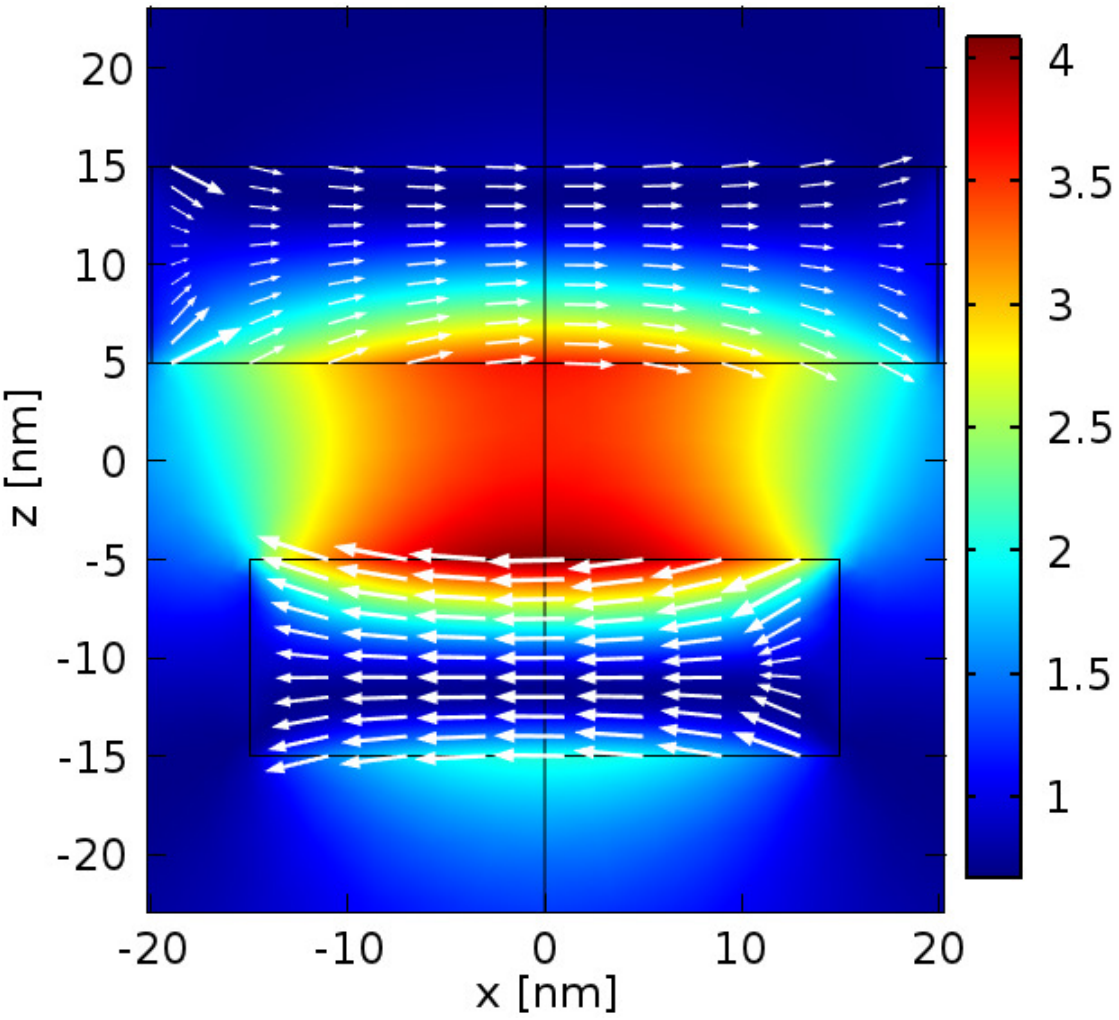

Figure 15: A silver metadimer in a two-dimensional square lattice of period $P = 50$ nm. The metadimers are embedded in glass and have the dimensions $(R_1,h_1,R_2,h_2,s) = (15,10,20,10,10)$, in nm. The illumination wavelength is $\lambda_0 = 618$ nm. Arrows: source current density vectors at $\omega t = \pi/2$. Colors: magnitude of the complex magnetic field normalized to that of the incident wave.

5 Summary and conclusions

The main goal of this work was to exploit the electromagnetic multipole expansion in characterizing electric current excitations in optical nanostructures. Motivated by the prospect of designing optical metamaterials for visible light, we studied subwavelength metallic scatterers, in which only a few low-order multipoles can be excited. We have found that the magnetic dipole and the electric quadrupole describe electric current excitations of the same order appearing in the same spectral range of the electromagnetic response of structures like metadimers. This result supports the findings described in Ref. [15].

In Sec. 2.4, we have shown that there are three different ways to calculate the multipole coefficients in the used multipole expansion. The method based on Eqs. (79) and (80), being the simplest to implement numerically, shows that the radial component of the electric or magnetic field determines whether the multipole is electric or magnetic. The method utilizing Eqs. (89) and (90), on the other hand, is the most general one, as it can be used to analyze the multipole excitations in an array of scatterers. We have derived Eqs. (89) and (90) in the form that does not include spatial derivatives of the source current density. This makes it easier to numerically evaluate the multipole coefficients.

In Sec. 3.1, we have introduced Eqs. (99), (110) and (111), which express the scattering, extinction and absorption cross sections of a single scatterer through the multipole coefficients. These expressions are generalizations of those which have previously been derived for spherical scatterers [17, 20]. We have found (see Sec. 4.2) that the individual terms in the summation in Eq. (99) can be interpreted as the modal scattering cross sections.

In Sec. 3.2, we have introduced the concept of a point current multipole to define a basis for the description of an arbitrary distribution of the electric current density in a meta-atom. We have derived Eqs. (158)-(160), which describe the electric current distributions giving rise to specific electric dipole, electric quadrupole and magnetic dipole radiations. Furthermore, we noted that in symmetric meta-atoms only the current quadrupoles Q_{xz} and Q_{zx} can be excited by x-polarized light.

In Secs. 3.3 and 3.4, we have presented a simple analytical description of the means by which a Q_{xz} current quadrupole moment can be excited in a metadimer. We have considered two closely spaced point scatterers with different electric dipole polarizabilities and studied the possibility to suppress the electric dipole excitation in them. In particular, we have rigorously proved that, if the electric dipole moment is reduced, the radiation from such an idealized metadimer is of a quadrupole character. We have also derived a criterion (Eq. (194)) for a dominant quadrupole scattering to be achieved.

In Sec. 4, we have used our multipole expansion to analyze the visible-light scattering by meta-atoms. For a silver-disc meta-atom, we have found that varying the disc radius between 15 and 20 nm considerably alters the spectral characteristics of the radiation. We have then combined two nanodiscs of different radii to form a disc metadimer and adjusted its geometry to suppress the electric dipole excitation. We have shown that within the spectral range of this electric dipole suppression,

the scattering is provided almost exclusively by the magnetic dipole and electric quadrupole modes.

In Sec. 4.3, we have described the interaction of light with 1D and 2D arrays of the silver disc metadimers. We have found that the electromagnetic coupling between the adjacent metadimers red-shifts the spectral location of the electric dipole suppression region, if the applied optical field is TM-polarized. Furthermore, the coupling was observed to further reduce the amplitude of the excited electric dipole moment. We have also found that the electric dipole suppression, and dominating magnetic dipole and electric quadrupole scattering, can always be realized within a certain spectral range for both one- and two-dimensional metadimer arrays.

In order to create a three-dimensional metamaterial, one can stack several layers of such two-dimensional metadimer arrays as considered here. For the resulting material to be homogeneous, the lattice period should be chosen as small as possible. We can, for example, introduce a 20 nm spacing between the adjacent layers and obtain a simple three-dimensional cubic lattice with a lattice constant of 50 nm. If in a certain spectral range, the material exhibits dominating quadrupole excitations in its unit cells, it can be called a quadrupole metamaterial. To our knowledge, this metamaterial design has not been previously presented in the literature. To describe the response of this material to light, one can perform spatial averaging of the microscopic Maxwell equations, in which the metadimers are treated as point multipoles, and obtain a new set of macroscopic Maxwell equations in which the material is considered as homogeneous. These equations will contain the macroscopic magnetization and quadrupole moment density as dominant terms in the constitutive relations at visible-light frequencies. Then, the reflection and refraction of light at an interface between the metamaterial and, say, a dielectric will not be determined by electric dipoles, but instead by electric quadrupoles and magnetic dipoles.

References

[1] R. E. Raab and O. L. De Lange, *Multipole Theory in Electromagnetism* (Oxford, New York, 2005).

[2] E. B. Graham and R. E. Raab, "Multipole solution for the macroscopic electromagnetic boundary conditions at a vacuum–dielectric interface", *Proc. R. Soc. Lond. A* **456**, 1193 (2000).

[3] E. B. Graham and R. E. Raab, "The role of the macroscopic surface density of bound electric dipole moment in reflection", *Proc. R. Soc. Lond. A* **457**, 471 (2001).

[4] W. Cai and V. Shalaev, *Optical Metamaterials: Fundamentals and Applications* (Springer, New York, 2009).

[5] V. G. Veselago, "The Electrodynamics of Substances with Simultaneously Negative Values of ϵ and μ", *Soviet Physics Uspekhi* **10**, 509 (1968).

[6] D. R. Smith, W. J. Padilla, D. C. Vier, S. C. Nemat-Nasser and S. Schultz, "Composite Medium with Simultaneously Negative Permeability and Permittivity", *Phys. Rev. Lett.* **84**, 4184 (2000).

[7] J. B. Pendry, A. J. Holden, D. J. Robbins and W. J. Stewart, "Magnetism from Conductors and Enhanced Nonlinear Phenomena", *IEEE Trans. Microwave Theory Tech.* **47**, 2075 (1999).

[8] J. Zhou, Th. Koschny, M. Kafesaki, E. N. Economou, J. B. Pendry and C. M. Soukoulis, "Saturation of the Magnetic Response of Split-Ring Resonators at Optical Frequencies", *Phys. Rev. Lett.* **95**, 223902 (2005).

[9] G. Dolling, C. Enkrich, M. Wegener, J. F. Zhou, C. M. Soukoulis and S. Linden, "Cut-wire pairs and plate pairs as magnetic atoms for optical metamaterials", *Opt. Lett.* **30**, 3198 (2005).

[10] A. N. Grigorenko, A. K. Geim, H. F. Gleeson, Y. Zhang, A. A. Firsov, I. Y. Khrushchev and J. Petrovic, "Nanofabricated media with negative permeability at visible frequencies", *Nature* **438**, 335 (2005).

[11] J. Valentine, S. Zhang, T. Zentgraf, E. Ulin-Avila, D. A. Genov, G. Bartal and X. Zhang, "Three-dimensional optical metamaterial with a negative refractive index", *Nature* **455**, 376 (2008).

[12] A. Alù, A. Salandrino and N. Engheta, "Negative effective permeability and left-handed materials at optical frequencies", *Opt. Express* **14**, 1557 (2006).

[13] C. Rockstuhl, F. Lederer, C. Etrich, T. Pertsch and T. Scharf, "Design of an Artificial Three-Dimensional Composite Metamaterial with Magnetic Resonances in the Visible Range of the Electromagnetic Spectrum", *Phys. Rev. Lett.* **99**, 17401 (2007).

[14] C. R. Simovski and S. A. Tretyakov, "Model of isotropic resonant magnetism in the visible range based on core-shell clusters", *Phys. Rev. B* **79**, 45111 (2009).

[15] D. J. Cho, F. Wang, X. Zhang and Y. R. Shen, "Contribution of the electric quadrupole resonance in optical metamaterials", *Phys. Rev. B* **78**, 121101 (2008).

[16] G. Russakoff, "A Derivation of the Macroscopic Maxwell Equations", *Am. J. Phys.* **38**, 1188 (1970).

[17] J. D. Jackson, *Classical Electrodynamics*, 3rd Ed. (Wiley, New York, 1999).

[18] L. D. Landau and E. M. Lifshitz, *Electrodynamics of Continuous Media* (Pergamon, Oxford, 1960).

[19] R. F. Harrington, *Time-Harmonic Electromagnetic Fields* (McGraw-Hill, New York, 1961).

[20] C. F. Bohren and D. R. Huffman, *Absorption and Scattering of Light by Small Particles*, 1st ed. (Wiley, New York, 1983).

[21] M. Born and E. Wolf, *Principles of Optics*, 7th Ed. (Cambridge, London, 2003).

[22] R. E. Raab and J. H. Cloete, "An eigenvalue theory of circular birefringence and dichroism in a non-magnetic chiral medium", *J. Electromagn. Waves Appl.* **8**, 1073 (1994).

[23] C. Rockstuhl, T. Zentgraf, E. Pshenay-Severin, J. Petschulat, A. Chipouline, J. Kuhl, T. Pertsch, H. Giessen and F. Lederer, "The origin of magnetic polarizability in metamaterials at optical frequencies - an electrodynamic approach", *Opt. Express* **15**, 8871 (2007).

[24] S. Tretyakov, *Analytical Modeling in Applied Electromagnetics* (Artech House, Boston, 2003).

[25] C. Menzel, T. Paul, C. Rockstuhl, T. Pertsch, S. Tretyakov and F. Lederer, "Validity of effective material parameters for optical fishnet metamaterials", *Phys. Rev. B* **81**, 35320 (2010).

[26] L. Novotny and B. Hecht, *Principles of Nano-Optics*. (Cambridge University Press, New York, 2006).

[27] R. Carminati, J.-J. Greffet, C. Henkel and J.M. Vigoureux, "Radiative and non-radiative decay of a single molecule close to a metallic nanoparticle", *Opt. Commun.* **261**, 368 (2006).

[28] T. J. Dufva, J. Sarvas and J. C.-E. Sten, "Unified derivation of the translational addition theorems for the spherical scalar and vector wave functions", *Progress In Electromagnetics Research B* **4**, 79 (2008).

[29] J. Henzie, J. Lee, M. H. Lee, W. Hasan and T. W. Odom, "Nanofabrication of Plasmonic Structures", *Annu. Rev. Phys. Chem.* **60**, 147 (2009).

[30] C. H. Liu, M. H. Hong, H. W. Cheung, F. Zhang, Z. Q. Huang, L. S. Tan and T. S. A. Hor, "Bimetallic structure fabricated by laser interference lithography for tuning surface plasmon resonance", *Opt. Express* **16**, 10701 (2008).

[31] H. Fredriksson, Y. Alaverdyan, A. Dmitriev, C. Langhammer, D. S. Sutherland, M. Zäch and B. Kasemo, "Hole-Mask Colloidal Lithography", *Adv. Mater.* **19**, 4297 (2007).

[32] P. B. Johnson and R. W. Christy, "Optical Constants of the Noble Metals", *Phys. Rev. B* **6**, 4370 (1972).

[33] T. Pakizeh, A. Dmitriev, M. S. Abrishamian, N. Granpayeh and M. Käll, "Structural asymmetry and induced optical magnetism in plasmonic nanosandwiches", *J. Opt. Soc. Am. B* **25**, 659 (2008).

[34] M. Abramowitz and I. A. Stegun, *Handbook of Mathematical Functions With Formulas, Graphs, and Mathematical Tables*, 10th ed. (U.S. Government Printing Office, 1972).

A Mathematical identities

A.1 Associated Legendre polynomial

The associated Legendre polynomial of degree l and order m is defined through the Rodrigues' formula [17]

$$P_l^m(\cos\theta) = \frac{(-1)^m}{2^l l!}(\sin\theta)^m \frac{d^{l+m}}{d(\cos\theta)^{l+m}}\big((\cos\theta)^2 - 1\big)^l. \tag{A1}$$

The orthogonality relation for P_l^m is

$$\int_0^\pi P_l^m(\cos\theta) P_p^m(\cos\theta)\sin\theta d\theta = \frac{2}{2l+1}\frac{(l+m)!}{(l-m)!}\delta_{lp}. \tag{A2}$$

The recurrence relations for P_l^m are [34]

$$(l-m)P_l^m(\cos\theta) = (2l-1)\cos\theta P_{l-1}^m(\cos\theta) - (l+m-1)P_{l-2}^m(\cos\theta), \tag{A3}$$

and

$$\frac{d}{d\theta}P_l^m(\cos\theta) = \frac{l\cos\theta P_l^m(\cos\theta) - (l+m)P_{l-1}^m(\cos\theta)}{\sin\theta}. \tag{A4}$$

The two equations above can be used to derive

$$\sin\theta\frac{d^2}{d\theta^2}P_l^m(\cos\theta) + \cos\theta\frac{d}{d\theta}P_l^m(\cos\theta) - m^2 P_l^m(\cos\theta)\frac{1}{\sin\theta} = -l(l+1)\sin\theta P_l^m(\cos\theta), \tag{A5}$$

which is the required expression for calculating the radial electric field from the multipole expansion in Sec. 2.4.

A.2 Useful integrals

The spherical harmonics include exponential functions of the form $e^{im\phi}$. The exponential functions have the orthogonality relations

$$\int_0^{2\pi} e^{i(m-n)\phi}d\phi = 2\pi\delta_{mn}, \tag{A6}$$

for any integers m and n. Operating with ∇ on the vector spherical harmonics often generates the angle-dependent functions

$$\tau_{lm}(\theta) = \frac{d}{d\theta}P_l^m(\cos\theta), \tag{A7}$$

and

$$\pi_{lm}(\theta) = \frac{m}{\sin\theta}P_l^m(\cos\theta). \tag{A8}$$

For these functions we have the following orthogonality relations

$$\int_0^\pi \big(\pi_{lm}(\theta)\pi_{pm}(\theta) + \tau_{lm}(\theta)\tau_{pm}(\theta)\big)\sin\theta d\theta = \delta_{lp}\frac{2l(l+1)}{2l+1}\frac{(l+m)!}{(l-m)!}, \tag{A9}$$

and

$$\int_0^\pi \big(\tau_{lm}(\theta)\pi_{pm}(\theta) + \tau_{pm}(\theta)\pi_{lm}(\theta)\big)\sin\theta d\theta = 0, \tag{A10}$$

for any integers $l \geq 0$, $p \geq 0$ and $-l \leq m \leq l$. The integral in Eq. (A10) can be proven by applying partial integration to one of the integrands and using the definition in Eq. (A1). To prove the result in Eq. (A9), we write the integrand as

$$\begin{aligned}\pi_{lm}\pi_{pm}\sin\theta + \tau_{lm}\tau_{pm}\sin\theta = \frac{1}{2}\big(l(l+1)+p(p+1)\big)P_l^m P_p^m \sin\theta + \\ \frac{1}{2}\frac{d}{d\theta}\big(\frac{dP_l^m}{d\theta}P_p^m\sin\theta + \frac{dP_p^m}{d\theta}P_l^m\sin\theta\big),\end{aligned} \tag{A11}$$

which can be verified by using Eq. (A5). The second part of the integrand yields 0. Applying Eq. (A2) to the first part of the integrand completes the proof.

A.3 Spherical Bessel functions

For the various radial functions, we follow the definitions used in Ref. [17]. The spherical Bessel functions are defined as

$$j_l(x) = \sqrt{\frac{\pi}{2x}}J_{l+1/2}(x), \tag{A12}$$

$$n_l(x) = \sqrt{\frac{\pi}{2x}}N_{l+1/2}(x), \tag{A13}$$

where J_l is the Bessel function of order l and N_l is the Neumann function of order l. The spherical Hankel functions of the first kind describe waves outgoing from the origin. They are defined as

$$h_l^{(1)}(x) = j_l(x) + in_l(x), \tag{A14}$$

The recurrence relations for $h_l^{(1)}$ are

$$h_{l-1}^{(1)}(x) + h_{l+1}^{(1)}(x) = \frac{2l+1}{x}h_l^{(1)}(x), \tag{A15}$$

and

$$\frac{d}{dx}h_l^{(1)}(x) = \frac{1}{2l+1}\big(lh_{l-1}^{(1)}(x) - (l+1)h_{l+1}^{(1)}(x)\big). \tag{A16}$$

The two equations above can be used to derive the equation

$$\frac{d}{dx}\Big(\frac{h_l^{(1)}(x)}{x^l}\Big) = -\frac{h_{l+1}^{(1)}(x)}{x^l}. \tag{A17}$$

The Riccati-Bessel functions are defined as

$$\Psi_l(x) = xj_l(x), \tag{A18}$$

$$\chi_l(x) = xn_l(x), \tag{A19}$$

$$\xi_l(x) = xh_l^{(1)}(x). \tag{A20}$$

Note that Ψ_l and χ_l are real valued functions, but ξ_l is not. We use a prime superscript to denote differentiation with respect to the argument, i.e., $\Psi_l'(x)$. The Wronskians of the Riccati-Bessel functions are [17]

$$\Psi_l(x)\chi_l'(x) - \chi_l(x)\Psi_l'(x) = 1, \tag{A21}$$

$$\Psi_l(x)\xi_l'(x) - \xi_l(x)\Psi_l'(x) = i, \tag{A22}$$

$$\chi_l(x)\xi_l'(x) - \xi_l(x)\chi_l'(x) = -1. \tag{A23}$$

Using Eqs. (A14) and (A21) we obtain

$$\xi_l'(x)\xi_l^*(x) = \Psi_l'(x)\Psi_l(x) + \chi_l'(x)\chi_l(x) + i, \tag{A24}$$

which is used for calculating the scattering cross section in Sec. 3.1.

A.4 Circular coordinates

We defined a circular coordinate system (w, w^*, z) such that

$$w = \frac{1}{\sqrt{2}}(x + iy), \tag{A25}$$

$$w^* = \frac{1}{\sqrt{2}}(x - iy). \tag{A26}$$

The z-coordinate is the same as in the Cartesian coordinates. The reverse transformation for the coordinates is

$$x = \frac{1}{\sqrt{2}}(w + w^*), \tag{A27}$$

$$y = -\frac{i}{\sqrt{2}}(w - w^*). \tag{A28}$$

To obtain a radius vector $\mathbf{r} = w\hat{\mathbf{w}} + w^*\hat{\mathbf{w}}^* + z\hat{\mathbf{z}}$, the unit vectors must be defined as $\hat{\mathbf{w}} = (\hat{\mathbf{x}} - i\hat{\mathbf{y}})/\sqrt{2}$ and $\hat{\mathbf{w}}^* = (\hat{\mathbf{x}} + i\hat{\mathbf{y}})/\sqrt{2}$. The reverse transformation for the unit vectors is

$$\hat{\mathbf{x}} = \frac{1}{\sqrt{2}}(\hat{\mathbf{w}} + \hat{\mathbf{w}}^*), \tag{A29}$$

$$\hat{\mathbf{y}} = \frac{i}{\sqrt{2}}(\hat{\mathbf{w}} - \hat{\mathbf{w}}^*). \tag{A30}$$

Any vector $\mathbf{v}$ can be written in the new system as $\mathbf{v} = v_w\hat{\mathbf{w}} + v_{w^*}\hat{\mathbf{w}}^* + v_z\hat{\mathbf{z}}$. Since $\hat{\mathbf{w}} \cdot \hat{\mathbf{w}} = 0$ and $\hat{\mathbf{w}} \cdot \hat{\mathbf{w}}^* = 1$, it follows that the w-component of a vector is

$$v_w = \mathbf{v} \cdot \hat{\mathbf{w}}^*, \tag{A31}$$

and likewise for the w^*-component. We see that complex conjugation is needed when projecting a vector on a complex coordinate axis.

The operator ∇ can also be written in the new coordinates. Consider ∇ operating on a function $f(w, w^*)$. Then the differentiation yields

$$\nabla f(w, w^*) = \hat{\mathbf{x}}\Big(\frac{df}{dw}\frac{dw}{dx} + \frac{df}{dw^*}\frac{dw^*}{dx}\Big) + \hat{\mathbf{y}}\Big(\frac{df}{dw}\frac{dw}{dy} + \frac{df}{dw^*}\frac{dw^*}{dy}\Big). \tag{A32}$$

Using Eqs. (A25), (A26), (A29) and (A30) in Eqs. (A32) yields

$$\begin{aligned}\nabla f(w,w^*) &= \frac{1}{2}(\hat{\mathbf{w}}+\hat{\mathbf{w}}^*)\Big(\frac{df}{dw}+\frac{df}{dw^*}\Big)-\frac{1}{2}(\hat{\mathbf{w}}-\hat{\mathbf{w}}^*)\Big(\frac{df}{dw}-\frac{df}{dw^*}\Big)\\ &= \hat{\mathbf{w}}\frac{df}{dw^*}+\hat{\mathbf{w}}^*\frac{df}{dw}.\end{aligned} \tag{A33}$$

This enables us to express the differentiation with respect to w as

$$\frac{d}{dw}f(\mathbf{r}) = \hat{\mathbf{w}}\cdot(\nabla f(\mathbf{r})), \tag{A34}$$

which is the projection of the gradient onto $\hat{\mathbf{w}}^*$. The nabla operator becomes

$$\nabla = \hat{\mathbf{w}}\frac{d}{dw^*}+\hat{\mathbf{w}}^*\frac{d}{dw}+\hat{\mathbf{z}}\frac{d}{dz} \tag{A35}$$

The coordinates w and w^* can be expressed in spherical coordinates as

$$w = \frac{r\sin\theta}{\sqrt{2}}e^{i\phi}, \tag{A36}$$

$$w^* = \frac{r\sin\theta}{\sqrt{2}}e^{-i\phi}. \tag{A37}$$

Likewise, the unit vectors $(\hat{\mathbf{w}},\hat{\mathbf{w}}^*,\hat{\mathbf{z}})$ can be expressed in spherical coordinates as

$$\hat{\mathbf{w}} = \frac{1}{\sqrt{2}}\big(\hat{\mathbf{r}}e^{-i\phi}\sin\theta+\hat{\theta}e^{-i\phi}\cos\theta-i\hat{\phi}e^{-i\phi}\big), \tag{A38}$$

$$\hat{\mathbf{w}}^* = \frac{1}{\sqrt{2}}\big(\hat{\mathbf{r}}e^{i\phi}\sin\theta+\hat{\theta}e^{i\phi}\cos\theta+i\hat{\phi}e^{i\phi}\big), \tag{A39}$$

$$\hat{\mathbf{z}} = \hat{\mathbf{r}}\cos\theta-\hat{\theta}\sin\theta. \tag{A40}$$